arXiv:astro-ph/9609093v1 13 Sep 1996

RESCEU-12/96, UTAP-241/96

SPIN-DOWN OF NEUTRON STARS AND COMPOSITIONAL TRANSITIONS IN THE COLD CRUSTAL MATTER

Kei Iida[1] and Katsuhiko Sato[1,2]

[1]Department of Physics, School of Science, the University of Tokyo
7-3-1 Hongo, Bunkyo, Tokyo 113, Japan;
iida@utaphp1.phys.s.u-tokyo.ac.jp, sato@phys.s.u-tokyo.ac.jp
[2]Research Center for the Early Universe, School of Science, the University of Tokyo
7-3-1 Hongo, Bunkyo, Tokyo 113, Japan

ABSTRACT

Transitions of nuclear compositions in the crust of a neutron star induced by stellar spin-down are evaluated at zero temperature. We construct a compressible liquid-drop model for the energy of nuclei immersed in a neutron gas, including pairing and shell correction terms, in reference to the known properties of the ground state of matter above neutron drip density, 4.3×10^{11} g cm^{-3}. Recent experimental values and extrapolations of nuclear masses are used for a description of matter at densities below neutron drip. Changes in the pressure of matter in the crust due to the stellar spin-down are calculated by taking into account the structure of the crust of a slowly and uniformly rotating relativistic neutron star. If the initial rotation period is $\sim$ ms, these changes cause nuclei, initially being in the ground-state matter above a mass density of about 3×10^{13} g cm^{-3}, to absorb neutrons in the equatorial region where the matter undergoes compression, and to emit them in the vicinity of the rotation axis where the matter undergoes decompression. Heat generation by these processes is found to have significant effects on the thermal evolution of old neutron stars with low magnetic fields; the surface emission predicted from this heating is compared with the *ROSAT* observations of X-ray emission from millisecond pulsars and is shown to be insufficient to explain the observed X-ray luminosities.

Subject headings: dense matter — nuclear reactions, nucleosynthesis, abundances — stars: interiors — stars: neutron — stars: rotation — X-rays: stars

1. INTRODUCTION

A neutron star crust consists of a lattice of nuclei embedded in a roughly uniform neutralizing background of electrons and, at densities above neutron drip, in a sea of neutrons. So far, properties of the ground-state matter in the crust, such as the nuclei present and the equation of state, have been well investigated on the basis of laboratory data on nuclei and many-body calculations of the properties of uniform nuclear matter (see, e.g., Pethick & Ravenhall 1995). If the crustal matter, initially in its ground state, is compressed or decompressed, the matter is expected to deviate from nuclear equilibrium; the constituents of matter, giving its lowest energy state, now turn into another ones. It is expected, furthermore, that the matter being out of nuclear equilibrium undergoes nuclear processes such as electron captures, $\beta-$decays, neutron absorption and emission, and nuclear fusion and fission; these processes can release nuclear energy to lower the total energy of the matter.

One of the astrophysical situations in which the pressure of matter in the crust is changing is in evolved neutron-star-black-hole binary systems; there may occur the tidal disruption of neutron stars by black holes. Lattimer et al. (1977) have investigated the compositions of expanding, initially cold, neutron star matter appropriate to these systems. It was noted that the compositions in the decompression bear a resemblance to those of hot r-process matter following a supernova explosion. Another situation is when a neutron star accretes matter from a companion star. If matter of $\sim 0.01M_\odot$ is accreted on to the surface of the star, the crust is composed totally of this accreted matter. Sato (1979) and Haensel & Zdunik (1990a) have examined the compositions of cold matter initially of a density of about 10^9 g cm^{-3} being compressed up to $\sim 10^{13}$ g cm^{-3}, which we may encounter in accreting neutron stars. Their conclusion was that the charge number of nuclei in the matter decreases as a result of electron captures and that, once neutrons drip out of the nuclei, the mass number also decreases by neutron emission. At the highest densities where Coulomb barrier between the nuclei is sufficiently low, pycnonuclear fusion was found to occur.

ROSAT observations of X-ray emission from rotation-powered pulsars give us important information on the surface emission from isolated (not accreting) neutron stars of various ages (Ögelman 1995). As the rotation is slowing down, the matter in the crust far away from the rotation axis is expected to be compressed due to decrease in the centrifugal force; on the other hand, the matter in the polar region may be decompressed due to increase in the length of the star along this axis. In this paper, we shall then investigate transitions of the nuclear compositions in the crust under such compression and decompression and effects of the release of nuclear energy on the thermal evolution of neutron stars.

During the time scale for the spin-down τ_s, which is $\gtrsim 10$ yr as deduced from a magnetic dipole braking, neutrino cooling processes work so effectively that the temperature of the crust is below $\sim 10^9$ K (see, e.g., Nomoto & Tsuruta 1987). For such temperatures, thermal energies are smaller than typical excitation energies of the system except in the outermost layers of the star where the thermal motion of electrons and ions affects the matter properties (Pethick & Ravenhall 1995). In describing matter in the crust of mass densities $\rho \gtrsim 10^9$ g cm^{-3} considered below, therefore, we assume its temperture to be zero. We also assume that this zero-temperature matter is in nuclear equilibrium before the compression and decompression proceed due to the spin-down.

Nuclear processes can occur in the cold crustal matter during the spin-down only when two conditions are satisfied. The first is that the time scale for the processes must be less than τ_s, and the second is that the Gibbs free energy of the system should be lowered by the processes. We first consider these criteria for electron captures, β-decays, and neutron absorption and emission. The time scale for neutron processes occurring above neutron drip density via the interactions of neutrons in continuum states with nuclei (Lattimer et al. 1977) is negligibly small compared with τ_s. According to the estimates made by Bisnovatyi-Kogan & Seidov (1970) and Lattimer et al. (1977), the time scale for β-processes, dependent on the nuclear structure and on the electron Fermi energies, may possibly be smaller than τ_s in the density region of interest to us, although this is still uncertain for the neutron-rich nuclei present near and above neutron drip density. The energy criterion for the occurrence of the processes considered may be re-expressed as the chemical potential of electrons (dripped neutrons) being across the energy threshold which is given by the difference in nuclear masses between before and after β-processes (neutron processes). Generally, this energy threshold depends strongly on *pairing and shell* effects in the nuclei, so that these effects should be duly taken into account in describing the nuclei in the crust. Next, let us inquire when nuclear fusion and fission can occur. The time scale for these processes is sensitive to the nuclear charge Z, since Z determines the size of Coulomb barrier between the nuclei and that of fission barrier (Lattimer et al. 1977; Sato 1979). Energetically, fusion and fission reactions can take place if the nuclear binding energy per nucleon becomes larger after these reactions. For both conditions, the occurrence of fusion and fission requires sufficiently small and large values of Z, respectively, compared with those for the equilibrium nuclei.

For the purpose of examining the chemical evolution of the neutron star crust as the star spins down, we construct a compressible liquid-drop model of nuclei in the inner crust (at densities above neutron drip) based on that of Baym, Bethe, & Pethick (1971; hereafter referred to as BBP) and use a description of matter in the outer crust (at densities below neutron drip) by Baym, Pethick, & Sutherland (1971; hereafter referred to as BPS). For the matter above neutron drip, not only is a nuclear surface energy term of BBP modified but also a shell correction term is added to the BBP expressions in such a way that the resulting compositions of the ground-state matter are consistent with those obtained by Negele & Vautherin (1973; hereafter referred to as NV) in their Hartree-Fock calculations of complete unit cells with an effective nucleon-nucleon interaction. A pairing correction term obtained by Möller & Nix (1992) as an empirical formula is also added to our nuclear model; an isospin dependence of nuclear pairing gaps found for laboratory nuclei was incorporated into their formula. Recent experimental values of the nuclear masses (Audi & Wapstra 1993) and their extrapolations (Möller et al. 1995) are built in the BPS expressions for the energy of matter below neutron drip. The resultant equation of state of the ground-state matter in the crust is found to be consistent with that of BPS. The next step is to calculate changes in the pressure of matter in the crust due to the stellar spin-down. We first describe the evolution of structure of the crust by using an equation of structure of a slowly and uniformly rotating relativistic star advanced by Hartle (1967) and the equation of state of BPS as well as by assuming a magnetic dipole spin evolution. Displacements of matter in the crust during the spin-down are then analyzed in the framework of general relativity. By comparing these displacements with the evolving pressure profile of the crust, we evaluate the variations in the pressure of the matter. Using the constructed nuclear model and the evaluated pressure variations as well as recalling the energy and time-scale conditions for the occurrence of nuclear processes described in the preceding paragraph, we investigate nuclear processes occurring in the crust during the spin-down, the resulting heat generation, and its effects on the thermal evolution of neutron stars.

In § 2, we first construct a model for zero-temperature matter in the crust, and we thereby calculate the compositions and equation of state of the matter in nuclear equilibrium. In § 3, a model for the crust of a neutron star that is rotating down is described; changes in the pressure of the crustal matter induced by the spin-down are calculated therefrom. In § 4, we evaluate transitions of the compositions of the zero-temperature matter, undergoing the changes in its pressure as calculated in § 3, from the equilibrium ones obtained in § 2. In § 5, a heating rate associated with these transitions is estimated, and its relation to the *ROSAT* observations of millisecond pulsars is examined. Conclusions are finally given in § 6.

2. MODELS FOR THE COLD CRUSTAL MATTER

In this section we construct an expression for the Gibbs free energy of zero-temperature matter in the neutron star crust. We then investigate the equilibrium nuclei present and the equation of state for these nuclei by minimizing the Gibbs free energy of the system under charge neutrality. We assume that the matter is composed of a single species of nucleus with nucleon number A and proton number Z at a given pressure P.

2.1. *Inner Crust*

A compressible liquid-drop model originally developed by BBP is useful for describing higher-energy states of cold matter in the inner crust on a footing equal to its ground state. BBP gave the energy $W_N(A, Z, V_N, n_n)$ of a spherical nucleus of volume V_N immersed in the uniform neutron gas of number density n_n as

$$W_N = [(1-x)m_n c^2 + x m_p c^2 + W(k,x)]A + W_{\rm Coul}(Z, V_N) + W_{\rm surf}^{\rm BBP}(A, Z, V_N, n_n)\ . \quad (1)$$

Here $m_n(m_p)$ is the neutron (proton) rest mass, $W(k,x)$ is the energy per nucleon for bulk nuclear matter of number density $n = 2k^3/3\pi^2 = A/V_N$ and of proton fraction $x = Z/A$ [see equation (3.19) of BBP], $W_{\rm Coul}(Z, V_N)$ is the Coulomb energy of protons distributed uniformly in the nucleus,

$$W_{\rm Coul} = \frac{3}{5}\frac{Z^2 e^2}{r_N} \quad (2)$$

with $r_N = (3V_N/4\pi)^{1/3}$, and $W_{\rm surf}^{\rm BBP}(A, Z, V_N, n_n)$ is the nuclear surface energy,

$$W_{\rm surf}^{\rm BBP} = \frac{\sigma[W(k_n,0) - W(k,x)]}{\omega_0}\left(1 - \frac{n_n}{n}\right)^{2/3} A^{2/3} \quad (3)$$

with $k_n = (3\pi^2 n_n/2)^{1/3}$, $\sigma = 21.0$ MeV, and $\omega_0 = 16.5$ MeV.

In the ground state of matter above neutron drip density, we take note of the nuclear charge obtained by NV in their Hartree-Fock (HF) calculations of complete unit cells. The Z values calculated by BBP agree fairly well with those by NV at mass densities

ρ between 4.3×10^{11} and 10^{13} g cm^{-3}, but significantly exceeds them with increasing density for $\rho \gtrsim 10^{13}$ g cm^{-3} (see Figure 6 of NV). Such behavior of Z is due to overestimation of the nuclear surface energy by BBP, which was clarified by Ravenhall, Bennett, & Pethick (1972; hereafter referred to as RBP) through comparison with their HF calculations of the surface energy with a Skyrme interaction. We thus affix to $W_{\rm surf}^{\rm BBP}$ a coefficient λ acting to reduce this surface energy:

$$\lambda = \begin{cases} 1 \ , & n_n = 0 \\ \tanh\left(\frac{C_1}{\mu_n}\right) \ , & n_n > 0 \ , \end{cases} \tag{4}$$

where

$$\mu_n = W(k_n, 0) + \frac{1}{3} k_n \frac{\partial W(k_n, 0)}{\partial k_n} \tag{5}$$

is the chemical potential of dripped neutrons (not including the rest mass), and C_1 is the adjustable parameter to be determined below. Hereafter we replace $W_{\rm surf}^{\rm BBP}$ in equation (1) by $W_{\rm surf}$ defined as $W_{\rm surf} = \lambda W_{\rm surf}^{\rm BBP}$ and refer to the equation thereby modified as equation (1)$'$.

The nuclear shell effects, giving rise to greater stability of the nuclei with neutron or proton magic numbers, also affect the charge number of the equilibrium nuclei; these effects were appropriately taken into account by NV through a proton spin-orbit force. We then add to equation (1)$'$ a shell correction term that was originally developed for isolated nuclei by Myers & Swiatecki (1966) and extended to nuclei in the dripped-neutron regime by Sato (1979):

$$\begin{aligned} W_{\rm shell} &= 5.8 \left\{ \frac{F(N, N_i)\chi + F(Z, Z_i)\chi + F(Z, Z_i')(1-\chi)}{(A/2)^{2/3}} \right. \\ &\qquad \left. -0.26[(1-x)\chi + x]A^{1/3} \right\} \text{MeV} \end{aligned} \tag{6}$$

with

$$F(X, M_i) = \frac{3}{5}\left[(M_i^{5/3} - M_{i-1}^{5/3}) \frac{X - M_{i-1}}{M_i - M_{i-1}} - (X^{5/3} - M_{i-1}^{5/3}) \right] \ , \ M_{i-1} \le X \le M_i \ , \tag{7}$$

$$\chi = \frac{1}{1 + \exp\left(\frac{\mu_n'}{C_2}\right)} \ , \tag{8}$$

where $N = A - Z$ is the number of neutrons in the nucleus, $N_i = \{2, 8, 14, 28, 50, 82, 126, 184, \cdots\}$ is the set of neutron magic numbers for isolated nuclei, $Z_i = \{2, 8, 14, 28, 50, 82, 114, \cdots\}$ is the set of proton magic numbers for isolated nuclei, $Z_i' = \{2, 8, 20, 28, 40, 50, 82, 114, \cdots\}$ is the set of proton magic numbers for nuclei in the external neutron gas found by NV, and

$$\mu_n' = \frac{\partial}{\partial A}[AW(k, x) + W_{\rm surf}(A, Z, V_N, n_n)]_{Z, V_N, n_n} \tag{9}$$

is roughly the chemical potential of neutrons in the nucleus. The factor χ ensures that equation (6) reproduces the empirical shell formula of Myers & Swiatecki (1966) for isolated nuclei, and that the dripped neutrons smear the neutron shells and turn the proton magic numbers Z_i into Z_i' (see Sato 1979).

The parameter C_2 has been determined together with C_1 in such a way as to reproduce the Z values of the ground-state matter calculated by NV at eleven mass densities, so that $C_1 = 5.5$ MeV and $C_2 = 0.1$ MeV. Strictly speaking, we have obtained $Z = 40$ in place of $Z = 32$ (NV) at the highest density. In this determination we have evaluated the values of Z by minimizing the Gibbs free energy of the system under charge neutrality, as will be discussed in § 2.3.

In Figure 1 we have compared the resultant surface tension, $E_s = W_{\rm surf}/4\pi r_N^2$, with the BBP and RBP results. The present values approach the HF values of RBP with increasing density (decreasing proton fraction) for $\rho \gtrsim 10^{13}$ g cm^{-3} ($x \lesssim 0.26$) and reproduce the BBP values in the density range 4.3×10^{11} g cm^{-3} $\leq \rho \lesssim 10^{13}$ g cm^{-3} ($0.26 \lesssim x \leq 0.31$). An improvement of the present surface energy over that of BBP has been thus clarified.

We next introduce the nuclear pairing effects, stabilizing the nuclei with even neutrons and even protons relative to the other types of nuclei, into the nuclear model hitherto determined by adding a pairing correction term obtained empirically by Möller & Nix (1992) in their macroscopic model:

$$W_{\rm pair} = \begin{cases} 0 & \text{(even-neutron, even-proton)} \\ \frac{r_{\rm MN} B_s}{N^{1/3}} {\rm e}^{-t_{\rm MN}\delta^2} & \text{(odd-neutron, even-proton)} \\ \frac{r_{\rm MN} B_s}{Z^{1/3}} {\rm e}^{-t_{\rm MN}\delta^2} & \text{(even-neutron, odd-proton)} \\ \frac{r_{\rm MN} B_s}{N^{1/3}} {\rm e}^{-t_{\rm MN}\delta^2} + \frac{r_{\rm MN} B_s}{Z^{1/3}} {\rm e}^{-t_{\rm MN}\delta^2} - \frac{h_{\rm MN}}{A^{2/3} B_s} & \text{(odd-neutron, odd-proton)} \end{cases} \qquad (10)$$

with $h_{\rm MN} = 6.6$ MeV, $r_{\rm MN} = 5.55$ MeV, and $t_{\rm MN} = 6.07$. Here $\delta = 1 - 2x$ is the relative neutron excess, and B_s is the surface area of a deformed nucleus divided by that of a spherical one. We simply set $B_s = 1$. It is to be noted that they determined $W_{\rm pair}$ from experimental mass differences in the isospin range $-0.1 < \delta < 0.25$, and that we shall extrapolate $W_{\rm pair}$ into the dripped-neutron regime ($0.4 \lesssim \delta \lesssim 0.7$). We also note that this pairing correction term, being measured relative to the even-even nuclei, produces no change in the charge number of the equilibrium nuclei.

We finally obtain the Gibbs free energy of the system above neutron drip per nucleon, as BBP did, according to

$$g = \frac{E_{\rm tot} + P}{n_N A_{\rm cell}} \qquad (11)$$

with

$$E_{\rm tot} = n_N m_N(A, Z, V_N, n_N, n_n) + \varepsilon_e(n_e) + (1 - n_N V_N)\varepsilon_n(n_n) \ , \qquad (12)$$

where $E_{\rm tot}$ is the total energy per unit volume, which is in turn related to ρ as $E_{\rm tot} = \rho c^2$, and n_N is the number of nuclei per unit volume. Here,

$$m_N = W_N(A, Z, V_N, n_n) + W_L(Z, V_N, n_N) + W_{\rm shell}(A, Z, V_N, n_n) + W_{\rm pair}(A, Z) \quad (13)$$

is the sum of the mass of a nucleus given by equations (1)′, (6), and (10) and the lattice energy in the Wigner-Seitz approximation,

$$W_L = -\frac{9}{10}\frac{Z^2e^2}{r_c}\left(1 - \frac{1}{3}\frac{r_N^2}{r_c^2}\right) \quad (14)$$

with $r_c = (3/4\pi n_N)^{1/3}$,

$$\varepsilon_e = \frac{m_e^4c^5}{8\pi^2\hbar^3}\{(2t^2+1)t(t^2+1)^{1/2} - \ln[t + (t^2+1)^{1/2}]\} \quad (15)$$

with $t = \hbar(3\pi^2 n_e)^{1/3}/m_e c$ is the energy of the free electron gas per unit volume,

$$\varepsilon_n = n_n[W(k_n, 0) + m_n c^2] \quad (16)$$

is the energy of the external neutron gas per unit volume, and

$$A_{\rm cell} = A + n_n\left(\frac{1}{n_N} - V_N\right) \quad (17)$$

is the nucleon number in a spherical Wigner-Seitz cell, which is equal to the ratio of the number density of baryons n_b to n_N.

2.2. *Outer Crust*

To construct a model of matter in the outer crust, we follow a line of arguments of BPS and set the Gibbs free energy of the system per nucleon as

$$g = \frac{E_{\rm tot} + P}{n_N A} \quad (18)$$

with

$$E_{\rm tot} = n_N m_N(A, Z, n_N) + \varepsilon_e(n_e)\ , \quad (19)$$

where ε_e is given by equation (15), and

$$m_N = M_N(A, Z) + W_L(Z, n_N) \quad (20)$$

is the sum of the mass of a nucleus $M_N(A,Z)$ and the energy of a bcc lattice,

$$W_L = -0.895929\frac{Z^2e^2}{r_c} \ . \tag{21}$$

Here the nuclear mass, not having the atomic-electron binding energy subtracted out, is related to the atomic mass $M_A(A,Z)$ as $M_N(A,Z) = M_A(A,Z) - Zm_ec^2$. The values of $M_A(A,Z)$ used here are taken from the experimental mass table of Audi & Wapstra (1993), when present. The masses of the remaining atoms are taken from the droplet (FRDM) mass table of Möller et al. (1995). We note that the matter model described above is the same as that of Haensel & Pichon (1994) except some minor differences concerning the electronic contribution to binding energies, the electron exchange energies, and the electron-screening effects.

2.3. *Ground-State Properties*

It is necessary to know the ground-state properties of matter in the crust for determining the initial model for the equation of state and the nuclear compositions. The equilibrium conditions for the matter are obtained by minimizing the Gibbs free energy per nucleon, g, given by equations (11) and (18) at fixed P under charge neutrality,

$$n_e = Zn_N \ . \tag{22}$$

For the matter in the inner crust, as investigated by BBP, the conditions for determining n_N and V_N at fixed P, A, Z, and n_n are the pressure equilibrium condition,

$$-\left.\frac{\partial m_N}{\partial V_N}\right|_{A,Z,n_N,n_n} = P^{(\mathrm{G})} \equiv \frac{1}{3}n_nk_n\frac{\partial W(k_n,0)}{\partial k_n} + \frac{n_nn_N}{1-V_Nn_N}\left.\frac{\partial m_N}{\partial n_n}\right|_{A,Z,V_N,n_N} \tag{23}$$

and the thermodynamic relation between P and n_b,

$$P = P^{(\mathrm{G})} + n_e^2\frac{\partial}{\partial n_e}\left(\frac{\varepsilon_e}{n_e}\right) + n_N^2\left.\frac{\partial W_L}{\partial n_N}\right|_{Z,V_N} \ . \tag{24}$$

The remaining conditions for determining A, Z, and n_n at fixed P, V_N, and n_N are the optimization of A in a nucleus,

$$S_{A+1} < \frac{\partial}{\partial A}\left(\frac{W_{\mathrm{Coul}} + W_{\mathrm{surf}} + W_L}{A}\right)_{x,n_NA,n_NV_N,n_n} < S_A \tag{25}$$

with

$$S_A = \frac{W_{\rm pair}(A-1,Z) + W_{\rm shell}\left(A-1, Z, \frac{A-1}{A}V_N, \frac{A}{A-1}n_N, n_n\right)}{A-1} - \frac{W_{\rm pair}(A,Z) + W_{\rm shell}(A,Z,V_N,n_N,n_n)}{A} \ , \tag{26}$$

the $\beta-$stability condition,

$$W_Z < \mu_e < W_{Z-1} \tag{27}$$

with

$$W_Z = m_N(A,Z,V_N,n_N,n_n) - m_N(A,Z+1,V_N,n_N,n_n) \ , \tag{28}$$

where $\mu_e = \partial\varepsilon_e/\partial n_e$ is the electron chemical potential including the rest mass, and the equilibrium of the dripped neutrons with the neutrons in a nucleus,

$$D_A < \mu_n + m_n c^2 < D_{A+1} \tag{29}$$

with

$$D_A = m_N(A,Z,V_N,n_N,n_n) - m_N\left(A-1, Z, V_N, n_N, n_n + \frac{n_N}{1-n_N V_N}\right) \ . \tag{30}$$

In the conditions (27) and (29), the quantities W_Z, W_{Z-1}, D_A, and D_{A+1} correspond to the energy thresholds necessary for $\beta-$decay, electron capture, neutron emission, and neutron absorption, respectively, to occur in a cell containing the nucleus (A, Z). We note that inequalities (25), (27), and (29) are only necessary conditions for determining the compositions of the ground-state matter; hence, we should find the parameters A, Z, and n_n, which give the minimum value of g, among those satisfying these inequalities.

For the matter in the outer crust, a complete description of the minimization of g is given by BPS. In this case, the equilibrium conditions (24) and (27) remain useful if we set $P^{(\rm G)} = 0$ and eliminate the parameters V_N and n_n.

The neutron drip point for the ground-state matter has been calculated by minimizing g given by equation (18) and finding the case in which $g = m_n c^2$, as evaluated by BPS. The result indicates that a neutron begins to drip out of ^{118}Kr at $\rho = 4.34 \times 10^{11}$ g cm^{-3}, $P = 4.93 \times 10^{-4}$ MeV fm^{-3}, and $\mu_e = 26.21$ MeV. The agreement with the results of BPS and of Haensel & Pichon (1994) has been thus confirmed.

Using the equilibrium conditions discussed above, we have obtained the equilibrium nuclear compositions for eleven cases of densities below neutron drip as well as for eleven cases of densities above neutron drip, which were chosen by NV, and determined the equation of state for these compositions; the result has been listed in Table 1. We have confirmed that the calculated nuclear compositions (including the chemical potentials

μ_e and μ_n) are consistent with those of Haensel & Pichon (1994) in the outer crust as well as those of NV in the inner crust. The equilibrium nuclear compositions listed in Table 1 will be used as the initial model for the nuclear compositions in § 4. As depicted in Figure 2, the equation of state in the present calculations agrees graphically with the equation of state of BPS which includes that of BBP in the dripped-neutron regime. We shall thus use the equation of state of BPS as that consistent with the present result for estimating the structure of the crust in § 3.

3. SPIN-DOWN AND CHANGES IN PRESSURE OF THE CRUSTAL MATTER

In this section we first construct a model for the crust of a zero-temperature neutron star rotating at a given angular velocity. By using a magnetic dipole approximation for the rotational evolution, the evolution of structure of the crust is determined. We finally estimate the displacements of elements of matter in the crust during the spin-down and then the corresponding changes in their pressures. We use units in which $c = G = 1$ in § 3.

3.1. *Model for the Crust of a Rotating Neutron Star*

As a first step towards the estimates of the changing pressures of matter in the crust during the spin-down, we consider a pressure profile of the crust of a neutron star that is in hydrostatic equilibrium and is rotating at a uniform angular velocity $\Omega = 2\pi/P_{\rm rot}$, where $P_{\rm rot}$ is the rotation period as seen by a distant observer. In a non-rotating equilibrium configuration, we assume the stellar mass M and radius R_s to be 1.4 $M_\odot$ and 10 km. We fix the total number of baryons in the star for arbitrary Ω. General relativistic effects on the crust model may be deduced from the following quantity included in the redshift factor at the surface of the non-rotating star:

$$\frac{2GM}{R_s c^2} \sim 0.4 \ . \qquad (31)$$

A fully general relativistic treatment of the configuration of the crust is thus required. If the star is rotating with $P_{\rm rot} = 1$ ms, being similar to the shortest period 1.6 ms among those observed from pulsars, the ratio between the typical magnitude of the rotational energy of the star and that of its gravitational potential is roughly

$$\frac{R_s^3\Omega^2}{2GM} \sim 0.1 \ . \tag{32}$$

We can then consider the rotation as a small perturbation on a non-rotating configuration. Consequently, we find that general-relativistic equations of structure of slowly and rigidly rotating stars obtained by Hartle (1967) exactly up to order Ω^2 are useful for our purpose of determining the pressure profile of the crust of a rotating neutron star.

Such a pressure profile may be obtained by determining the transformation of a surface of constant pressure in the equilibrium configuration of the crust of a neutron star rotating at a given Ω from a spherical one of radius R in the non-rotating equilibrium configuration subject to conservation of the number of baryons in the star. We denote the position of the surface of constant pressure in the rotating configuration by the ordinary polar coordinates r and θ in which the polar axis is taken to be the rotation axis. At a given θ, the radius of the surface may be written as (Hartle 1967)

$$r = R + \xi(R,\theta) + \mathrm{O}(\Omega^4) \ , \tag{33}$$

where

$$\xi(R,\theta) = \xi_0(R) + \xi_2(R)P_2(\cos\theta) \tag{34}$$

is the displacement of order Ω^2 from its non-rotating position. Here $\xi_0(R)$ denotes the change in the mean radius of the surface, and $\xi_2(R)P_2(\cos\theta)$ represents the quadrupolar deformation of the surface, where $P_2(\cos\theta)$ is the second-order Legendre polynomial. For the present purpose, we should then evaluate the radius R of the surface of constant pressure in the configuration of the non-rotating neutron star crust and its displacement $\xi(R,\theta)$ due to the rotation.

We first calculate the pressure profile, $P(R)$, of the crust of a non-rotating neutron star by using the equation of state of BPS in the Tolman-Oppenheimer-Volkoff (TOV) equations (see Shapiro & Teukolsky 1983):

$$\frac{dP(R)}{dR} = -\frac{[\rho(R)+P(R)][m(R)+4\pi R^3P(R)]}{R^2}\mathrm{e}^{-\nu(R)} \ , \tag{35}$$

where

$$\mathrm{e}^{\nu(R)} = 1 - \frac{2m(R)}{R} \tag{36}$$

with

$$m(R) = M - \int_R^{R_s} dr 4\pi r^2 \rho(r) \tag{37}$$

is the redshift factor. The pressure profile $P(R)$ obtained by solving equation (35) inward from the surface of the star is shown in Figure 3, together with the density profile $n_b(R)$. Here we have assumed that the crust dissolves into uniform nuclear matter at a density of ≈ 0.1 fm^{-3}, as suggested by Lorenz, Ravenhall, & Pethick (1993).

We proceed to estimate the displacement, $\xi(R,\theta)$, of the surface of constant pressure in the crust from the non-rotating one due to the rotation, using the results for this displacement obtained by Hartle (1967) and Hartle & Thorn (1968). Since the thickness of the crust is small compared with R_s as depicted in Figure 3, it can be assumed that $\xi(R,\theta) \approx \xi(R_s,\theta)$ throughout the crust. To calculate the displacement of the surface of the star $\xi(R_s,\theta)$, we note the solutions of Einstein's field equations for a perfect fluid in the gravitational field of the rotating configuration that is characterized by the metric having the following form up to order Ω^2 (Hartle 1967):

$$\begin{aligned} ds^2 &= -\mathrm{e}^{\nu(r)}\{1+2[h_0(r)+h_2(r)P_2(\cos\theta)]\}(dx^0)^2 \\ &\quad +\mathrm{e}^{-\nu(r)}\left\{1+\frac{2[m_0(r)+m_2(r)P_2(\cos\theta)]}{r-2m(r)}\right\}dr^2 \\ &\quad +r^2\{1+2[v_2(r)-h_2(r)]P_2(\cos\theta)\}\{d\theta^2+\sin^2\theta[d\phi-\omega(r)dx^0]^2\}\ , \end{aligned} \tag{38}$$

where $\nu(r)$ and $m(r)$ are given by equations (36) and (37). At the surface of the star, the solutions for the first- and second-order quantities contained in equation (38) are obtained by Hartle (1967) as

$$\omega(R_s) = \frac{2J}{R_s^3} \tag{39}$$

$$h_0(R_s) = -\frac{\delta M}{R_s\left(1-\frac{2M}{R_s}\right)} + \frac{J^2}{R_s^4\left(1-\frac{2M}{R_s}\right)} \tag{40}$$

$$h_2(R_s) = \frac{J^2}{MR_s^3}\left(1+\frac{M}{R_s}\right) + \frac{5}{8M^3}\left(Q-\frac{J^2}{M}\right)Q_2{}^2\left(\frac{R_s}{M}-1\right) \tag{41}$$

$$m_0(R_s) = \delta M - \frac{J^2}{R_s^3} \tag{42}$$

$$m_2(R_s) = (R_s-2M)\left[-h_2(R_s)+\frac{6J^2}{R_s^4}\right] \tag{43}$$

$$v_2(R_s) = -\frac{J^2}{R_s^4} + \frac{5}{4M^3}\frac{MQ-J^2}{\sqrt{R_s(R_s-2M)}}Q_2{}^1\left(\frac{R_s}{M}-1\right)\ , \tag{44}$$

where J is the total angular momentum of the star related to the moment of inertia I of the star as $J = I\Omega$, δM is the change in mass of the star from its non-rotating value, Q is the quadrupole moment of the star, and ${Q_2}^m$ is the associated Legendre polynomial of the second kind. At fixed baryon number, δM is given by (Hartle 1970)

$$\delta M = \frac{1}{2} I \Omega^2 \ . \tag{45}$$

The quantity of $\xi_2(R_s)$ can be derived from the integral of the equation of hydrostatic equilibrium for the rotating configuration [see equations (28), (89), and (91) of Hartle (1967)] as

$$\xi_2(R_s) = -\left\{ \frac{1}{3} \frac{R_s^2[\Omega - \omega(R_s)]^2}{1 - \frac{2M}{R_s}} + h_2(R_s) \right\} \frac{R_s^2}{M} \left(1 - \frac{2M}{R_s}\right) \ . \tag{46}$$

The parameters which still remain to be determined are I, Q, and $\xi_0(R_s)$. These values, dependent on the properties of neutron star matter, have been taken on the basis of the results for the rotating configuration at a stellar mass of about 1.4 $M_\odot$ obtained by Hartle & Thorn (1968), using the V_γ equation of state that is hard rather than soft, as

$$I = 10^{45} \text{ g cm}^{-3} \tag{47}$$

$$Q = 0.04 \left(\frac{\Omega}{\Omega_0}\right)^2 M R_s^2 \tag{48}$$

$$\xi_0(R_s) = 0.06 \left(\frac{\Omega}{\Omega_0}\right)^2 R_s \ , \tag{49}$$

where Ω_0 is the angular velocity at $P_{\rm rot} = 1$ ms. Here we have taken into account differences between the rotations at fixed central density and the rotations at fixed baryon number, the former being assumed by Hartle & Thorn (1968). We have thus obtained

$$\frac{\xi(R_s, \theta)}{R_s} = (-0.039 + 0.149 \sin^2\theta) \left(\frac{\Omega}{\Omega_0}\right)^2 \ . \tag{50}$$

Equation (50), as well as the solutions of the TOV equations obtained by using the equation of state of BPS, gives the present model for the crust of a neutron star rotating at a given Ω.

In Figure 4 we have drawn the surface of the star derived from equation (50) at $\Omega = \Omega_0$ together with the surface of radius R_s at $\Omega = 0$. We observe in this comparison that the rotation acts to shorten (enlarge) the surface of the star in the polar (equatorial) region.

3.2. *Rotational and Structural Evolution*

We assume that the evolution of the rotation of the star is determined by the usual magnetic-dipole model for pulsars (see Shapiro & Teukolsky 1983) as

$$\Omega(t)=\frac{\Omega(t=0)}{\sqrt{1+\frac{\Omega(t=0)^2B^2R_s^6}{3Ic^3}t}}\ . \tag{51}$$

Here B is the constant magnetic-dipole field at the magnetic pole of the star which is taken to be on the equator, and t denotes the age of the star. The constant B is then expressed in terms of the rotation period $P_{\rm rot}$ and its derivative $\dot{P}_{\rm rot}$ as $B\approx\sqrt{10^{39}P_{\rm rot}\dot{P}_{\rm rot}}$; the values of B that are determined by the quantities $P_{\rm rot}$ and $\dot{P}_{\rm rot}$ observed from pulsars range from $\sim10^8$ G to $\sim10^{12}$ G (Taylor, Manchester, & Lyne 1993). By using equation (51), the time scale for the spin-down may be estimated as $\tau_s\sim6\times10^5[10^{10}{\rm G}/B({\rm G})]^2[\Omega_0/\Omega(t=0)]^2$ yr.

Let us now ask how the structure of the crust is varying as the rotation of the star is slowing down according to equation (51). We assume that the total number of baryons in the star remains constant during the spin-down, and that the star is in hydostatic equilibrium and is rotating rigidly at $t=0$. Since the period derivative $\dot{P}_{\rm rot}$ observed from pulsars is extremely small (typically 10^{-15} s s^{-1}), the configuration of the star can be considered to maintain its hydrostatic equilibrium and rigid rotation. Then, the displacement of the surface of the star given by equation (50) as well as the perturbative quantities given by equations (39)–(44) may be redetermined at a given t as $\xi(R_s,\theta,t)$, $\omega(R_s,t)$, etc., by substituting $\Omega(t)$ into Ω included in each equation. In addition, we neglect the variation in the equation of state of matter in the crust during the spin-down, an assumption to be justified by calculating the equation of state of the matter deviating from its ground state in § 4. The evolution of structure of the crust is thus described in terms of the quantity $\xi(R_s,\theta,t)$ and of the pressure profile of the non-rotating configuration obtained by using the equation of state of BPS.

3.3. *Changes in the Pressure of the Crustal Matter*

For our main purpose of investigating transitions of the compositions of the cold crustal matter during the spin-down, it is essential to calculate the Lagrangian changes in pressure associated with elements of matter in the crust. Such Lagrangian changes in pressure may be obtained by combining the displacements of matter elements from their initial positions with the Eulerian changes in pressure obtained in § 3.2. For convenience, we denote the initial position of a matter element by the depth Δr, the distance measured from the surface of the star along the radial line, and by the polar angle θ. We then express the position of this element at a given t by the depth $\Delta r+\eta(\Delta r, \theta, t)$ and the polar angle $\theta+\alpha(\Delta r, \theta, t)$, as shown in Figure 5. The quantities η and α correspond to the displacements in the radial and angular directions between the element and an observer who is initially located at the same point as the element and is comoving with the surface of constant pressure in the radial direction.

The direction in which elements of matter in the crust move as the star is spinning down gives the relation between the quantities η and α. Let us assume that the direction of movement of an element present at (r, θ, t) is parallel to the sum of the gravitational and centrifugal forces acting on the element. In the hydrostatic equilibrium configuration considered here, these forces are in balance with the pressure gradient. As can be seen from the radius of the surface of constant pressure given by equation (33), the θ component of the pressure gradient is of order Ω^2, whereas the r component is of zeroth order. We thus find α to be of order Ω^4, by comparison with η of order Ω^2. Consequently, the quantity α can be neglected within the framework of the present perturbative treatment.

To find the quantity $\eta(\Delta r, \theta, t)$, we note that each element of matter in the crust is to be identified by counting the number of baryons inward from the surface of the star along the radial line. This identification may be made by following the baryon number conservation law (see Misner & Sharp 1964) according to

$$\begin{aligned} &\int_{R_s-\Delta r}^{R_s} dR \sin\theta \left\{ r^2 \mathrm{e}^{-\frac{\nu(r)}{2}} [1+\Delta(r,\theta,t=0)] \right\}_{r=R+\xi(R_s,\theta,t=0)} n_b(R) \\ &= \int_{R_s-\Delta r-\eta(\Delta r,\theta,t)}^{R_s} dR \sin\theta \left\{ r^2 \mathrm{e}^{-\frac{\nu(r)}{2}} [1+\Delta(r,\theta,t)] \right\}_{r=R+\xi(R_s,\theta,t)} n_b(R) \ , \end{aligned} \tag{52}$$

where $n_b(R)$ is the density profile of the non-rotating configuration shown in Figure 3, and

$$\Delta(r,\theta,t) = \frac{(\sqrt{-g}u^0)_{r,\theta,t}}{r^2 \mathrm{e}^{-\frac{\nu(r)}{2}} \sin\theta} - 1 \tag{53}$$

is the factor of order Ω^2 determined by the determinant g of the metric of equation (38) and by the time component of the 4-velocity of the matter,

$$\begin{aligned} u^0(r,\theta,t) \ &= \ \mathrm{e}^{-\frac{\nu(r)}{2}} \left\{ 1 + \frac{1}{2} r^2 \mathrm{e}^{-\nu(r)} [\Omega(t) - \omega(r,t)]^2 \sin^2\theta - h_0(r,t) - h_2(r,t) P_2(\cos\theta) \right\} \\ &\quad + \mathrm{O}(\Omega^4) \ . \end{aligned} \tag{54}$$

We then set $\Delta(r, \theta, t) \approx \Delta(R_s, \theta, t)$ in equation (52), by noting the correspondence with the approximation, $\xi(R, \theta, t) \approx \xi(R_s, \theta, t)$, available for thin crusts as discussed in § 3.1. The values of $\Delta(R_s, \theta, t)$ can be calculated from equations (36), (38), (39), (41)–(44), (54) as

$$\begin{aligned}
\Delta(R_s, \theta, t) &= \frac{1}{2}\mathrm{e}^{-\nu(R_s)} R_s^2 \{[\Omega(t) - \omega(R_s, t)]^2 - \omega(R_s, t)^2\} \sin^2\theta \\
&\quad +2[v_2(R_s, t) - h_2(R_s, t)]P_2(\cos\theta) + \frac{m_0(R_s, t) + m_2(R_s, t)P_2(\cos\theta)}{R_s - 2M} \\
&= (-0.043 + 0.094 \sin^2\theta) \left[\frac{\Omega(t)}{\Omega_0}\right]^2 . \qquad (55)
\end{aligned}$$

We have thus obtained the quantity $\eta(\Delta r, \theta, t)$ by retaining only the terms of order Ω^2 in equation (52) as

$$\begin{aligned}
\eta(\Delta r, \theta, t) &= \left[\frac{\mathrm{e}^{\frac{\nu(R)}{2}}}{R^2 n_b(R)}\right]_{R=R_s-\Delta r} \\
&\quad \times \left\{[\Delta(R_s, \theta, t=0) - \Delta(R_s, \theta, t)] \int_{R_s-\Delta r}^{R_s} dR R^2 \mathrm{e}^{-\frac{\nu(R)}{2}} n_b(R) \right. \\
&\quad \left. + [\xi(R_s, \theta, t=0) - \xi(R_s, \theta, t)] \int_{R_s-\Delta r}^{R_s} dR \frac{d}{dR}\left[R^2 \mathrm{e}^{-\frac{\nu(R)}{2}}\right] n_b(R)\right\} . \\
&\qquad (56)
\end{aligned}$$

We now turn to the evaluations of changes in the pressure of matter in the crust induced by the spin-down. Recall the definition of $\eta(\Delta r, \theta, t)$ shown in Figure 5 and the evolving pressure profile of the crust described in § 3.2. Then, the change until an age t in the pressure of an element that is initially located at the point denoted by Δr and θ may be written as

$$\begin{aligned}
\delta P(\Delta r, \theta, t) &= P(R)|_{R=R_s-\Delta r-\eta(\Delta r,\theta,t)} - P(R)|_{R=R_s-\Delta r} \\
&= -\eta(\Delta r, \theta, t)\left[\frac{dP(R)}{dR}\right]_{R=R_s-\Delta r} + \mathrm{O}(\Omega^4) , \qquad (57)
\end{aligned}$$

where $P(R)$ is the pressure profile of the non-rotating configuration shown in Figure 3. We have calculated the values of $\eta(\Delta r, \theta, t)$ according to equation (56), and, by substituting these values into equation (57), we have obtained the values of $\delta P(\Delta r, \theta, t)$. The result has been expressed as

$$\frac{\delta P(\Delta r, \theta, t)}{P(R_s - \Delta r)} = (-0.11 + 0.35 \sin^2\theta) \frac{\Omega(t=0)^2 - \Omega(t)^2}{\Omega_0^2} . \qquad (58)$$

Here we have omitted the Δr dependence of $\delta P(\Delta r, \theta, t)/P(R_s - \Delta r)$, since it makes negligible differences.

Figure 6 illustrates as a function of θ the values of $\delta P(\Delta r, \theta, t \to \infty)/P(R_s - \Delta r)$ given by equation (58) in which we set $P_{\rm rot}(t = 0) = 1$ ms; this quantity denotes the change in the pressure of an element of the crustal matter at an age of far later than τ_s divided by its initial pressure. We thus see that the matter is compressed in the equatorial region of the crust and is decompressed in the polar region due to the spin-down, as noted in § 1.

4. TRANSITIONS OF NUCLEAR COMPOSITIONS IN THE CRUST

Let us consider nuclear processes induced in the cold crustal matter, initially in nuclear equilibrium, by the changes in its pressure due to the spin-down as discussed in the preceding section. We first ask how the matter being compressed or decompressed departs from its ground state in which the system satisfies the equilibrium conditions (23)–(25), (27), and (29). We note that the time scale for pressure readjustment, corresponding to the sound travel time across a nucleus (Lattimer et al. 1977), is negligibly small compared with the spin-down time scale τ_s, so that the system should always satisfy the pressure conditions (23) and (24). Due to the assumption that the system contains a single species of nucleus at a given pressure, we may replace the condition (25) by the condition that the number of baryons, $A_{\rm cell}$, in a single cell remains constant. If nuclear fusion (fission) were to occur, however, this process would double (halve) the value of $A_{\rm cell}$. The conditions (27) and (29) ensure stability of the matter against $\beta-$ and neutron processes, respectively. While one of these processes is in progress, the system, not satisfying the corresponding stability condition, is out of quasi-equilibrium. Here we note that the time scale for neutron processes is far shorter than τ_s, and we assume that the time scale for $\beta-$processes is also smaller than τ_s. Then, the system may be considered to retain quasi-equilibrium during the spin-down. We shall thus pay attention only to the energy criterion for the occurrence of nuclear processes in analyzing the chemical evolution of the crust.

By noting the Gibbs free energy of the system per nucleon given by equations (11) and (18) as well as the conditions to be satisfied in the compression and decompression as discussed above, we have examined transitions of the composition of a unit cell from the equilibrium one listed in Table 1 due to the change in its pressure during the spin-down as follows: (i) At each pressure shifting from the equilibrium value $P_{\rm eq}$, we have calculated the Gibbs free energy per nucleon under the charge neutrality (22) and the pressure conditions (23) and (24) for the initial nuclide $(A, Z, A_{\rm cell})$ as well as for the nuclides $(A, Z \pm 1, A_{\rm cell})$, $(A \pm 1, Z, A_{\rm cell})$, $(2A, 2Z, 2A_{\rm cell})$, and $(A/2, Z/2, A_{\rm cell}/2)$, resulting from β-processes, neutron processes, fusion, and fission, respectively. (ii) By finding the case in which the Gibbs free energy for the nuclide arising from the reactions becomes equal to the energy for the initial one, we have determined the type of reaction expected to occur first and its threshold pressure $P_{\rm th}$. (iii) At the pressure equal to $P_{\rm th}$, we have determined the transitions to the next nuclides according to the criterion that the Gibbs free energy calculated for the nuclide present after the reactions under the conditions (22)–(24) should be lower than that for the previous one, until the system attains quasi-equilibrium. (iv) By following a line similar to (i)–(iii), we have examined a series of processes expected to occur with a further change in pressure. In (i)–(iv) we have assumed that, if β- and neutron processes were energetically possible at the same time, neutron processes would go first.

In addition to the changes in the nuclear compositions, we have evaluated the nuclear energy q thereby released per nucleon according to the thermodynamics at zero temperature as $q = g_i - g_f$, where g_i is the Gibbs free energy per nucleon for the nuclide before the reactions, and g_f is that for the next nuclide. As far as $\beta-$ and neutron processes are concerned, not only the reactions which release no energy but those which release some can take place. If the Fermi energies of electrons (dripped neutrons) become equal to the energy thresholds for $\beta-$ (neutron) processes during the compression or decompression, the electrons (neutrons) at the sea levels disappear or come out without supplying the medium with energy. Since these reactions proceed in a quasi-equilibrium condition, we shall refer to such processes as quasi-equilibrium processes. On the other hand, the reactions can liberate some energy when the Fermi energies of electrons (dripped neutrons) are in excess of the energy thresholds for electron captures (neutron absorption), i.e., $\mu_e > W_{Z-1}$ $(\mu_n + m_n c^2 > D_{A+1})$, as well as when those are below the energy thresholds for $\beta-$decays (neutron emission), i.e., $\mu_e < W_Z$ $(\mu_n + m_n c^2 < D_A)$. In the former case, the electrons (dripped neutrons) with energy between W_{Z-1} (D_{A+1}) and μ_e $(\mu_n + m_n c^2)$ are captured by the nuclei, which leads to excitation of the nuclei and to creation of holes in the electron (neutron) Fermi sphere. In the latter case, the nuclei add the electrons (neutrons) with energy between μ_e $(\mu_n + m_n c^2)$ and W_Z (D_A) to the electron (neutron) Fermi sea and simultaneously undergo excitation. In both cases, therefore, the reactions reduce the system to a non-equilibrium state; hereafter we shall denote such processes by non-equilibrium processes. At zero temperature considered here, the following relaxation towards quasi-equilibrium results in liberation of the energy $qA_{\rm cell}$ per unit cell; for neutron absorption, neutron emission, electron captures, and $\beta-$decays, $qA_{\rm cell} \approx \mu_n + m_n c^2 - D_{A+1}$,

$qA_{\rm cell} \approx D_A - \mu_n - m_n c^2$, $qA_{\rm cell} \approx \mu_e - W_{Z-1}$, and $qA_{\rm cell} \approx W_Z - \mu_e$, respectively. The relaxation processes involved, the resulting heat generation, and the applicability of the zero-temperature approximation will be discussed in § 5.

We proceed to show the results for the transitions from the equilibrium nuclides to the other ones during the compression of matter in the equatorial region of the crust due to the spin-down. The increase in its pressure can amount to about 24% for $P_{\rm rot}(t = 0) = 1$ ms as shown in Figure 6. In Figure 7 we have drawn the diagrams that show the changes in nuclides induced by such or a little larger increase in pressure from six equilibrium nuclides present at mass densities $\rho_{\rm eq}$ above neutron drip.

In the initial density region 4.3×10^{11} g cm^{-3} $\leq \rho_{\rm eq} \lesssim 3 \times 10^{13}$ g cm^{-3}, as shown in Figures 7a–7c, electron captures occur first when $P = P_{\rm th}$, at which the electron chemical potential μ_e, increasing due to the compression, attains the energy threshold W_{Z-1}. These processes are quasi-equilibrium ones. Thereafter, a succession of neutron emission and electron captures takes place at the same pressure as non-equilibrium processes. This result indicates that the nuclei undergoing non-equilibrium neutron emission (electron captures) have energy thresholds D_A (W_{Z-1}) larger (smaller) than $\mu_n + m_n c^2$ (μ_e) in contrast with the initial nuclei. This contrast is partly because the initial nuclei have even proton and neutron numbers and hence receive greater stability from the pairing effects, which are described by equation (10), and partly because they have closed shells of protons leading to local energy minima, which are determined by equation (6). A quasi-equilibrium state, in which the system includes the even-even nuclei in most cases, follows this series of reactions and lasts until the pressure arrives at the threshold for the forthcoming electron captures.

For initial densities of about 3×10^{13} g cm^{-3}, neutron absorption begins to take place along with β-processes as a result of the increase in the chemical potential of dripped neutrons during the compression, as can be seen from Figure 7d. This result implies that, at such initial densities, the nuclei are immersed in the neutron gas dense enough for the threshold pressure for neutron absorption to become comparable to that for electron captures. For higher initial densities up to about 2×10^{14} g cm^{-3}, as shown in Figures 7e and 7f, neutron absorption rather than electron captures occurs first as quasi-equilibrium processes when $P = P_{\rm th}$ at which $\mu_n + m_n c^2 \approx D_{A+1}$. These processes are accompanied by neutron absorption which occurs at the same pressure in a non-equilibrium condition and hence releases some nuclear energy. The resulting state in which the system contains the even-even nuclei remains in quasi-equilibrium, until further increase in pressure leads to the next two-stage neutron absorption. The two-step feature of the reactions stems from the fact that the energy thresholds D_{A+1}

depend on the parity of the reacting nuclei due to the nuclear pairing effects; this feature can be observed schematically from Figure 8a.

At initial densities below neutron drip, it is shown that electron captures take place first at the threshold pressure higher than $P_{\rm eq}$ by more than 40%. Such increment in pressure, however, is larger than that expected from the compression due to the spin-down. This result suggests that the energy thresholds for electron captures, W_{Z-1}, formed mainly by the closed shells of neutrons (protons for Ni) and pairing gaps in the equilibrium nuclei present in this density regime (see Table 1) are large enough to keep the nuclei stable against the reactions during the spin-down.

As can be observed from the results mentioned above, no fusion reaction is allowed energetically by the compression during the spin-down in the whole density region of the crust. This is because electron captures, leading to a reduction in the nuclear charge, do not proceed sufficiently for the occurrence of fusion.

We now summarize the nuclear processes expected to occur in the compressed matter during the spin-down and the energies thereby released. By comparing the threshold pressure $P_{\rm th}$ for the processes occurring first (see Figure 7) with the pressure to be increased by the spin-down with $P_{\rm rot}(t = 0) = 1$ ms in the equatorial region of the crust (see Figure 6), we find that, when $P_{\rm rot}(t = 0) \gtrsim 1$ ms, almost all the processes occurring in the compression are neutron absorption by the nuclei initially present in the density region 3×10^{13} g cm^{-3} $\lesssim \rho_{\rm eq} \lesssim 2 \times 10^{14}$ g cm^{-3}. In Table 2 we have shown the changes in the nuclear compositions in such a density regime with increasing pressure up to 24% and the energy q released per nucleon. We see that both the ratio of $P_{\rm th}$ to $P_{\rm eq}$ shown in Figure 7 and the energy released by non-equilibrium neutron absorption as listed in Table 2 tend to decrease as the initial density (proton fraction) increases (decreases), a feature coming primarily from the isospin dependence of $W_{\rm pair}$ given by equation (10).

For the purpose of examining the change in the equation of state of the compressed matter from the equilibrium one during the spin-down, we have also calculated the equation of state for the compositions of matter which are altered from the equilibrium ones listed in Table 1 by an increase of 30% in pressure. Figure 9 depicts the resulting equation of state, together with the equilibrium equation of state listed in Table 1 and with the equation of state of BPS. We observe in this figure that the non-equilibrium equation of state, as well as the equilibrium one, agrees graphically with that of BPS in the nearly whole density region. Such agreement between the non-equilibrium and BPS equations of state may justify our neglecting effects of the variation in the equation of state during the spin-down on the structure of the crust, as noted in § 3.2. It is interesting to notice the deviation of the non-equilibrium equation of state from the equilibrium one found for densities between 4.3×10^{11} and 3×10^{12} g cm^{-3}. Such deviation originates from the fact that the threshold effects prevent neutron emission, leading to softening of the equation of state in this density range, from proceeding enough for the number density of dripped neutrons n_n to reach its equilibrium value at the same pressure, as suggested by Haensel & Zdunik (1990b).

We conclude this section by showing the results for the changing compositions of the decompressed matter in the polar region of the crust during the spin-down. We have found that, basically, the processes occurring in the decompression are inverse processes against those caused by the compression in the whole density regime. This result is due to the fact that the electron and external neutron gases, controlling the occurrence of β- and neutron processes, undergo a reduction in their chemical potentials during the decompression in contrast with the case during the compression. For $P_{\rm rot}(t = 0) = 1$ ms, Figure 6 shows that the pressure of the matter in the vicinity of the rotation axis decreases by about 11% during the spin-down. In consequence of such decrease in pressure, neutron emission is found to take place as two-stage reactions composed of a quasi-equilibrium process and a non-equilibrium one at initial densities between 5×10^{13} and 2×10^{14} g cm^{-3}. Figure 8b depicts a schematic of nuclear levels relevant to these two-stage reactions. In Table 3 we have shown the changes in the nuclear compositions in such a density regime with decreasing pressure down to 11% and the energy per nucleon released by neutron emission. In comparison with Table 2, we observe that the changes in nuclides during the decompression and those during the compression from the same equilibrium nuclides are analogous with each other in terms of the energy release and of the pressure intervals between the adjacent thresholds for the reactions.

5. HEAT GENERATION AND NEUTRON STAR THERMAL EVOLUTION

The energies released by neutron absorption and emission that occur during the compression and decompression turn completely into heat through relaxation processes such as scattering between neutrons in the continuum states and γ de-excitation of the reacting nuclei. The heat thereby deposited locally in the substance is ~ 0.1 MeV per reaction, which is in turn carried away by electrons through their scattering with phonons, impurities, and other electrons (Flowers & Itoh 1976). The time scale for the heat conduction across a unit cell can be estimated as $\tau_H \sim c_P r_c^2/\kappa$, where c_P is the specific heat per unit volume at constant pressure, which is simply assumed to be the sum of that for the degenerate nonrelativistic neutrons of density n_n and that for the degenerate relativistic electrons of density n_e, and κ is the thermal conductivity. We then note that the time interval, τ_I, between when the pressure reaches the threshold for the reaction in a cell and when in the neighboring cell is $\sim \tau_s r_c/\eta$, where η is given by equation (56). At typical densities and temperatures of the substance around the reacting cell, $c_P \sim 10^{20}$ erg K^{-1} cm^{-3}, $\kappa \sim 10^{20}$ erg cm^{-1} K^{-1} s^{-1}, $r_c \sim 10$ fm, and $\eta \sim 10$ m, so that $\tau_H \ll \tau_I$. We can thus assume that the heat production by the reaction in a cell makes no change in the energy criterion for the reactions occurring next in the surrounding cells, which has been designed at zero temperature in § 4, and hence in the results shown in Tables 2 and 3 for the chemical evolution of the crust.

The total heat, $Q_{\rm tot}$, deposited in the star during the spin-down with $P_{\rm rot}(t=0)=1$ ms may be estimated from the following: (i) The energy per unit volume released by a non-equilibrium neutron process that occurs in the matter initially present at densities between 3×10^{13} and 2×10^{14} g cm^{-3} (0.02 fm$^{-3}\lesssim n_b \lesssim 0.1$ fm^{-3}) is evaluated from Tables 2 and 3 as $n_b q \approx 4$ eV fm^{-3}, irrespective of densities. (ii) The reacting material is initially located at the interior of depths Δr between 450 and 700 m, as can be seen from Figure 3. (iii) The number of the non-equilibrium processes, $N(\Delta r)$, occurring during the spin-down in a unit cell that is initially located at the depth Δr on the equatorial plane is estimated from Table 2 and Figure 3 as $N(\Delta r) \approx 15(\Delta r - r_1)/(r_2 - r_1)$, $r_1 < \Delta r < r_2$, where $r_1 = 450$ m and $r_2 = 700$ m. (iv) The ratio between the number of the non-equilibrium processes taking place on the cone of fixed θ and that on the equatorial plane is $\approx \sin\theta|1-1.46\cos^2\theta|$ as deduced from equation (58). By using (i)–(iv) and by taking account of the redshift effect on energy generation inside the non-rotating star (Thorn 1977), we have roughly estimated $Q_{\rm tot}$ as

$$\begin{aligned} Q_{\rm tot} &\approx \frac{2\pi R_s^2 n_b q}{\sqrt{1-\frac{2GM}{R_s c^2}}} \int_{r_1}^{r_2} d\Delta r N(\Delta r) \int_0^{\pi} d\theta \sin\theta |1-1.46\cos^2\theta| \\ &\approx 10^{46}\ \text{erg}\ . \end{aligned} \tag{59}$$

This value of $Q_{\rm tot}$ is found to be smaller than the initial rotational energy of the star, $I\Omega_0^2/2$, by six orders of magnitude; therefore, $Q_{\rm tot}$ has negligible effects on the rotational evolution determined by the magnetic dipole braking.

We now consider a heating rate $H(t)$, the heat deposited in the star by the non-equilibrium neutron processes that occur per unit time at an age t. Note that both the pressure intervals between the adjacent thresholds for the non-equilibrium reactions occurring in a unit cell and the energies thereby released take on almost constant values, as can be seen from Tables 2 and 3. Then, we may assume that the heat generated until a given age is proportional to the variation in the pressure of the reacting material due to the spin-down until that age as described by equation (58). We thus obtain

$$\int_0^t H(t')dt' = \frac{Q_{\rm tot}[\Omega(t=0)^2 - \Omega(t)^2]}{\Omega_0^2} \ . \tag{60}$$

Consequently, the heating rate may be expressed as

$$\begin{aligned} H(t) &\approx 5\times 10^{-7}\dot{E}(t) \\ &\approx 5\times 10^{32} \frac{\left[\frac{B({\rm G})}{10^{10}{\rm G}}\right]^2 \frac{\Omega(t=0)^4}{\Omega_0^4}}{\left\{1+1.54\left[\frac{B({\rm G})}{10^{10}{\rm G}}\right]^2 \frac{\Omega(t=0)^2}{\Omega_0^2}\frac{t({\rm yr})}{10^6{\rm yr}}\right\}^2} \ {\rm erg\ s^{-1}} \ , \end{aligned} \tag{61}$$

where

$$\dot{E}(t) = -I\Omega(t)\dot{\Omega}(t) \tag{62}$$

is the spin-down power derived from equation (51).

To ascertain the practical utility of equation (61), we recall that the occurrence of neutron processes in the crustal matter requires the changes of at least a few percent in its pressure, as seen from Tables 2 and 3. In consequence, the condition for use of equation (61) is roughly estimated from equation (58) as

$$\Omega(t=0)^2 - \Omega(t)^2 \gtrsim 0.1\Omega_0^2 \ . \tag{63}$$

We thus see that the present heating mechanism works when $P_{\rm rot}(t=0) \lesssim 3$ ms and $t \gtrsim 0.1\tau_s$.

Figure 10 illustrates as a function of the age the heating rate given by equation (61) in which $P_{\rm rot}(t=0) = 1$ ms and $B = 10^8, 10^9, 10^{10}, 10^{11}, 10^{12}$ G. The age at which $H(t)$ starts to decline remarkably corresponds to the spin-down time scale τ_s. We first consider the age of up to $\sim 10^6$ yr when neutrino emission from the interior of the star dominates over photon emission from the surface (see, e.g., Nomoto & Tsuruta 1987). In the light of models for the neutron star thermal evolution including some heating sources (see, e.g., Cheng et al. 1992; Reisenegger 1995; Van Riper, Link, & Epstein 1995), we expect that, at such times, the present heating source inside the stars even with high magnetic fields $\sim 10^{12}$ G does not contribute to the surface emission considerably compared with the contribution of the initial cooling of the stars. For $t > 10^6$ yr, on the other hand, it is generally predicted that the heat deposited initially is gone, and that the surface emission, dominant over the neutrino emission, is controlled entirely by some heat generation inside the star. It is noteworthy in Figure 10 that the heating rate for $B \sim 10^8$ G lasts during a term far longer than

10^6 yr. We thus see that the old neutron stars with low magnetic fields, characteristic of millisecond pulsars, are the most significant examples in investigating effects of the present heating mechanism on the neutron star thermal evolution.

In Figure 11 we have depicted the bolometric and X-ray (0.1–2.4 keV) luminosities, $L_{\rm bol}^H$ and L_X^H, predicted from the heating rate (61) as a function of the spin-down power $\dot{E}$, together with the X-ray luminosities obtained from the *ROSAT* observations of some millisecond pulsars in the energy range $0.1 - 2.4$ keV (Danner, Kulkarni, & Thorsett 1994) and with an empirical formula for X-ray luminosities coming from the stellar magnetosphere as proposed by Ögelman (1995). Here we have evaluated the bolometric luminosity $L_{\rm bol}^H$ by assuming a complete balance between the photon emission from the surface of the star and the heat production inside the star as well as by taking into account the redshift effect on the surface emission in the configuration of the non-rotating star (Thorn 1977) as

$$L_{\rm bol}^H = H\left(1 - \frac{2GM}{R_s c^2}\right) \ . \tag{64}$$

The X-ray luminosity L_X^H has been then obtained by assuming a spectrum of the emission from a spherical blackbody of radius R_s having the uniform surface temperature as observed by a distant spectator (Nomoto & Tsuruta 1987):

$$T_s^\infty = \left(\frac{L_{\rm bol}^H}{4\pi\sigma_{\rm SB}R_s^2}\right)^{1/4}\left(1 - \frac{2GM}{R_s c^2}\right)^{1/4} \ , \tag{65}$$

where $\sigma_{\rm SB}$ is the Stefan-Boltzmann constant. We have selected the pulsars satisfying the condition (63) among those chosen by Danner et al. (1994).

We observe in Figure 11 that the X-ray luminosities of millisecond pulsars are far larger than L_X^H. In comparison with the empirical result for magnetospheric X-ray luminosities obtained by Ögelman (1995), however, the X-ray luminosities observed are predicted to contain a large amount of nonthermal magnetospheric component in addition to a thermal component. We may thus conclude that the heat deposited in the star by neutron absorption and emission during the spin-down contributes little to the X-ray luminosities from millisecond pulsars; such a contribution is buried in the other components such as the magnetospheric one.

6. CONCLUSIONS

We have calculated the changes in the pressure of zero-temperature matter in the crust of an isolated rotating neutron star during its spin-down and the resulting transitions of the compositions of the matter initially in nuclear equilibrium. We have found that the matter is compressed and decompressed in the equatorial and polar regions of the crust, respectively, as the rotation of the star is slowing down. The corresponding change in the equation of state has been shown to have negligible effects on the structure of the crust. Through the compression (decompression), the nuclei initially present at densities between 3×10^{13} and 2×10^{14} g cm^{-3} have been found to absorb (emit) neutrons, when $P_{\rm rot}(t = 0) \lesssim 3$ ms. The heating rate arising from these processes has been estimated; we have clarified its marked effects on the thermal evolution of old neutron stars with low magnetic fields of $\sim 10^8$ G. It has been shown that the X-ray (0.1–2.4 keV) luminosity predicted from the present heating mechanism is far smaller than the values observed from millisecond pulsars.

The uncertainty affecting the occurrence of nuclear processes, which has been found in the dripped-neutron regime, stems primarily from the present extrapolation of the empirical formula for nuclear pairing gaps to higher relative neutron excess δ, as noted in § 2, and possibly from the omission of pairing correlations in the external neutron gas. Fortunately, the pairing effects in the neutron gas, leading to stabilization of the continuum states of neutrons, would be insensitive to the energy thresholds for reactions, to which, however, the pairing correlations between nucleons inside a nucleus are crucial. We expect that the validity of the extrapolation used here will be confirmed by microscopic calculations of the pairing gaps in the nuclei far from the β-stability valley with a realistic nucleon-nucleon interaction.

Another problem which remains to be investigated is the detailed description of the transition from roughly spherical nuclei in the external neutron gas to uniform nuclear matter. Lorenz et al. (1993) and Oyamatsu (1993) discovered that the phases containing nuclei of nonspherical (cylindrical or planar) shapes may exist at densities lower than the point at which the matter becomes uniform. If so, these nuclear shapes, affecting the discrete states of nucleons inside a nucleus, may have nonnegligible consequences for the occurrence of nuclear processes and hence for the heat generation.

We are grateful to Dr. T. Takatsuka and Dr. Y. Furihata for useful discussion and comments. This work was supported in part by Grants-in-Aid for Scientific Research provided by the Ministry of Education, Science, and Culture of Japan through Research

Grants Nos. 05243103 and 07CE2002.

TABLE 1

Properties of the Ground-State Matter in the Crust

P (MeV fm^{-3})	ρ (g cm^{-3})	n_b (fm^{-3})	Z	A	$A_{\rm cell}$	x	μ_e (MeV)	μ_n (MeV)
		outer		*crust*				
4.000×10^{-7}	1.496×10^{9}	9.005×10^{-7}	28	66	66.	0.42	4.459	0
1.000×10^{-6}	3.022×10^{9}	1.819×10^{-6}	36	86	86.	0.42	5.598	0
5.000×10^{-6}	1.041×10^{10}	6.259×10^{-6}	34	84	84.	0.40	8.338	0
1.000×10^{-5}	1.812×10^{10}	1.089×10^{-5}	32	82	82.	0.39	9.902	0
3.000×10^{-5}	4.293×10^{10}	2.578×10^{-5}	30	80	80.	0.38	13.01	0
8.000×10^{-5}	9.349×10^{10}	5.608×10^{-5}	28	78	78.	0.36	16.61	0
1.000×10^{-4}	1.150×10^{11}	6.897×10^{-5}	44	126	126.	0.35	17.63	0
1.500×10^{-4}	1.605×10^{11}	9.874×10^{-5}	42	124	124.	0.34	19.50	0
2.000×10^{-4}	2.055×10^{11}	1.231×10^{-4}	40	122	122.	0.33	20.95	0
3.000×10^{-4}	2.882×10^{11}	1.725×10^{-4}	38	120	120.	0.32	23.17	0
4.300×10^{-4}	3.914×10^{11}	2.342×10^{-4}	36	118	118.	0.31	25.34	0
		inner		*crust*				
5.012×10^{-4}	4.667×10^{11}	2.791×10^{-4}	40	130	139.7	0.31	26.29	0.124
5.635×10^{-4}	6.692×10^{11}	3.999×10^{-4}	40	130	189.5	0.31	26.79	0.388
6.828×10^{-4}	1.004×10^{12}	6.000×10^{-4}	40	132	263.1	0.30	27.48	0.648
8.746×10^{-4}	1.472×10^{12}	8.791×10^{-4}	40	134	354.7	0.30	28.26	0.919
1.483×10^{-3}	2.663×10^{12}	1.589×10^{-3}	40	136	547.9	0.29	29.78	1.434
4.055×10^{-3}	6.257×10^{12}	3.730×10^{-3}	50	180	1156.	0.28	33.23	2.461
7.346×10^{-3}	9.684×10^{12}	5.770×10^{-3}	50	186	1412.	0.27	35.96	3.179
1.371×10^{-2}	1.497×10^{13}	8.913×10^{-3}	50	194	1627.	0.26	39.65	4.069
4.746×10^{-2}	3.432×10^{13}	2.040×10^{-2}	50	218	1834.	0.23	50.20	6.448
0.1777	8.010×10^{13}	4.749×10^{-2}	40	220	1417.	0.18	67.32	10.38
0.4094	1.334×10^{14}	7.890×10^{-2}	40	282	1300.	0.14	82.06	14.09

TABLE 2

Nuclear Compositions in the Inner Crust during the Compression

P (MeV fm^{-3})	$P/P_{\rm eq}$	ρ (g cm^{-3})	Z	A	$A_{\rm cell}$	μ_e (MeV)	μ_n (MeV)	q (keV)
0.04746[a]	1	3.432×10^{13}	50	218	1834.	50.07	6.448	
0.05410	1.14	3.739×10^{13}	49	218	1834.	51.31	6.767	0.000
0.05700	1.20	3.867×10^{13}	49	219	1834.	51.89	6.896	0.000
0.05700	1.20	3.869×10^{13}	49	220	1834.	51.90	6.896	0.000
0.05700	1.20	3.864×10^{13}	50	220	1834.	52.22	6.889	0.043
0.05766	1.21	3.896×10^{13}	49	220	1834.	52.02	6.923	0.000
0.1777[a]	1	8.010×10^{13}	40	220	1417.	67.32	10.38	
0.1881	1.06	8.293×10^{13}	40	221	1417.	68.10	10.60	0.000
0.1881	1.06	8.293×10^{13}	40	222	1417.	68.10	10.60	0.096
0.1947	1.10	8.473×10^{13}	40	223	1417.	68.59	10.74	0.000
0.1947	1.10	8.473×10^{13}	40	224	1417.	68.59	10.73	0.093
0.2014	1.13	8.654×10^{13}	40	225	1417.	69.07	10.87	0.000
0.2014	1.13	8.654×10^{13}	40	226	1417.	69.07	10.87	0.090
0.2082	1.17	8.833×10^{13}	40	227	1417.	69.54	11.01	0.000
0.2082	1.17	8.833×10^{13}	40	228	1417.	69.54	11.00	0.088
0.2151	1.21	9.012×10^{13}	40	229	1417.	70.01	11.14	0.000
0.2151	1.21	9.015×10^{13}	40	230	1417.	70.01	11.14	0.086
0.4094[a]	1	1.334×10^{14}	40	282	1300.	82.06	14.09	
0.4232	1.03	1.360×10^{14}	40	283	1300.	82.58	14.26	0.000
0.4232	1.03	1.360×10^{14}	40	284	1300.	82.58	14.26	0.050
0.4315	1.05	1.375×10^{14}	40	285	1300.	82.89	14.37	0.000
0.4315	1.05	1.375×10^{14}	40	286	1300.	82.89	14.37	0.049
0.4396	1.07	1.390×10^{14}	40	287	1300.	83.19	14.47	0.000
0.4396	1.07	1.390×10^{14}	40	288	1300.	83.19	14.47	0.049
0.4477	1.09	1.405×10^{14}	40	289	1300.	83.48	14.57	0.000
0.4477	1.09	1.405×10^{14}	40	290	1300.	83.48	14.57	0.048
0.4560	1.11	1.420×10^{14}	40	291	1300.	83.78	14.67	0.000
0.4560	1.11	1.421×10^{14}	40	292	1300.	83.79	14.67	0.048
0.4641	1.13	1.435×10^{14}	40	293	1300.	84.07	14.77	0.000
0.4641	1.13	1.435×10^{14}	40	294	1300.	84.07	14.77	0.046
0.4720	1.15	1.449×10^{14}	40	295	1300.	84.35	14.86	0.000
0.4720	1.15	1.450×10^{14}	40	296	1300.	84.36	14.86	0.046
0.4801	1.17	1.464×10^{14}	40	297	1300.	84.63	14.96	0.000
0.4801	1.17	1.464×10^{14}	40	298	1300.	84.63	14.96	0.044
0.4878	1.19	1.478×10^{14}	40	299	1300.	84.89	15.05	0.000
0.4878	1.19	1.478×10^{14}	40	300	1300.	84.89	15.05	0.043
0.4962	1.21	1.493×10^{14}	40	301	1300.	85.18	15.15	0.000
0.4962	1.21	1.493×10^{14}	40	302	1300.	85.18	15.15	0.043
0.5042	1.23	1.507×10^{14}	40	303	1300.	85.43	15.24	0.000
0.5042	1.23	1.507×10^{14}	40	304	1300.	85.44	15.24	0.042

[a] Initial equilibrium nuclides.

TABLE 3

NUCLEAR COMPOSITIONS IN THE INNER CRUST DURING THE DECOMPRESSION

P (MeV fm^{-3})	$P/P_{\rm eq}$	ρ (g cm^{-3})	Z	A	$A_{\rm cell}$	$\mu_{\rm e}$ (MeV)	$\mu_{\rm n}$ (MeV)	q (keV)
0.1777[a]	1	8.010×10^{13}	40	220	1417.	67.32	10.38	
0.1662	0.94	7.688×10^{13}	40	219	1417.	66.41	10.13	0.000
0.1662	0.94	7.684×10^{13}	40	218	1417.	66.40	10.13	0.100
0.1598	0.90	7.499×10^{13}	40	217	1417.	65.86	9.985	0.000
0.1598	0.90	7.497×10^{13}	40	216	1417.	65.86	9.985	0.103
0.4094[a]	1	1.334×10^{14}	40	282	1300.	82.06	14.09	
0.3941	0.96	1.305×10^{14}	40	281	1300.	81.46	13.88	0.000
0.3941	0.96	1.304×10^{14}	40	280	1300.	81.44	13.88	0.051
0.3862	0.94	1.289×10^{14}	40	279	1300.	81.13	13.78	0.000
0.3862	0.94	1.289×10^{14}	40	278	1300.	81.13	13.78	0.053
0.3784	0.92	1.274×10^{14}	40	277	1300.	80.81	13.67	0.000
0.3784	0.92	1.273×10^{14}	40	276	1300.	80.80	13.67	0.054
0.3705	0.90	1.258×10^{14}	40	275	1300.	80.47	13.56	0.000
0.3705	0.90	1.257×10^{14}	40	274	1300.	80.46	13.56	0.055

[a] Initial equilibrium nuclides.

REFERENCES

Audi, G., & Wapstra, A. H. 1993, Nucl. Phys., A565, 1

Baym, G., Bethe, H. A., & Pethick, C. J. 1971, Nucl. Phys., A175, 225

Baym, G., Pethick, C. J., & Sutherland, P. 1971, ApJ, 170, 299

Bisnovatyi-Kogan, G. S., & Seidov, Z. F. 1970, Soviet Astron., 14, 113

Cheng, K. S., Chau, W. Y., Zhang, J. L., & Chau, H. F. 1992, ApJ, 396, 135

Danner, R., Kulkarni, S. R., & Thorsett, S. E. 1994, ApJ, 436, L153

Flowers, E., & Itoh, N. 1976, ApJ, 206, 218

Haensel, P., & Pichon, B. 1994, A&A, 283, 313

Haensel, P., & Zdunik, J. L. 1990a, A&A, 227, 431

———. 1990b, A&A, 229, 117

Hartle, J. B. 1967, ApJ, 150, 1005

———. 1970, ApJ, 161, 111

Hartle, J. B., & Thorn, K. S. 1968, ApJ, 153, 807

Lattimer, J. M., Mackie, F., Ravenhall, D. G., & Schramm, D. N. 1977, ApJ, 213, 225

Lorenz, C. P., Revenhall, D. G., & Pethick, C. J. 1993, Phys. Rev. Lett., 70, 379

Misner, C. W., & Sharp, D. 1964, Phys. Rev., 136, B571

Möller, P., & Nix, J. R. 1992, Nucl. Phys., A536, 20

Möller, P., Nix, J. R., Myers, W. D., & Swiatecki, W. J. 1995, At. Data Nucl. Data Tables, 59, 185

Myers, W. D., & Swiatecki, W. J. 1966, Nucl. Phys., 81, 1

Negele, J. W., & Vautherin, D. 1973, Nucl. Phys., A207, 298

Nomoto, K., & Tsuruta, S. 1987, ApJ, 312, 711

Ögelman, H. 1995, in The Lives of the Neutron Stars, ed. M. A. Alpar, Ü. Kiziloğlu, & J. van Paradijs (Kluwer: Dordrecht), 101

Oyamatsu, K. 1993, Nucl. Phys., A561, 431

Pethick, C. J., & Ravenhall, D. G. 1995, Annu. Rev. Nucl. Part. Sci., 45, 429

Ravenhall, D. G., Bennett, C. D., & Pethick, C. J. 1972, Phys. Rev. Lett., 28, 978

Reisenegger, A. 1995, ApJ, 442, 749

Sato, K. 1979, Prog. Theor. Phys., 62, 957

Shapiro, S. L., & Teukolsky, S. A. 1983, Black Holes, White Dwarfs, and Neutron Stars (New York: Wiley)

Taylor J. H., Manchester, R. N., & Lyne, A. G. 1993, ApJS, 88, 529

Thorn, K. S. 1977, ApJ, 212, 825

Van Riper, K. A., Link, B., & Epstein, R. I. 1995, ApJ, 448, 294

FIGURE CAPTIONS

FIG. 1.— The surface tension as a function of x, the proton fraction in nuclei. The solid curve is the result obtained in the present calculations, the dotted curve is the BBP result, and the dashed curve is the RBP result.

FIG. 2.— Equation of state of the crustal matter in its ground state. The solid circles denote the present result, and the line is the BPS result.

FIG. 3.— Pressure and density profiles of the crust of a non-rotating neutron star of mass 1.4 $M_\odot$ and radius 10 km, as calculated from the equation of state of BPS. The solid line is the pressure P (in MeV fm^{-3}), and the dashed line is the number density of baryons n_b (in fm^{-3}). The distances R and Δr (in km) are measured from the center and surface of the star, respectively. We have set the density at which the phase with nuclei changes into the liquid phase as ≈ 0.1 fm^{-3}; the depth Δr at this phase boundary is represented by the dotted line $\Delta r = r_2$, where $r_2 = 700$ m. The dotted line $\Delta r = r_1$, where $r_1 = 450$ m, corresponds to the depth at a density $n_b \approx 0.02$ fm^{-3}.

FIG. 4.— Surfaces of a neutron star in the rotating and non-rotating configurations at fixed total baryon number. The solid curve is the surface of the star rotating at a rotation period of 1 ms, and the dashed curve is the surface of the non-rotating star of radius 10 km. The z axis is taken to be the rotation axis.

FIG. 5.— Definition of the quantities η and α, denoting the position of an element of matter in the crust at an age t (open circle). Its initial position (solid circle) is denoted by Δr and θ. The surface (a) is the surface of a neutron star rotating at an angular velocity $\Omega(t)$.

FIG. 6.— The change in the pressure of an element of matter in the crust at an age when the rotation decays completely, being divided by its initial pressure, as a function of the polar angle denoting its position. The initial rotation period $P_{\rm rot}(t = 0)$ is taken to be 1 ms.

FIG. 7.— Changes in nuclides due to increase in pressure at initial densities above neutron drip. The solid circles are the initial equilibrium nuclides at a density $\rho_{\rm eq}$ and a pressure $P_{\rm eq}$. The crosses are the nuclides in the matter being in quasi-equilibrium.

The pressures $P_{\rm th}$ are the threshold ones for the reactions occurring first.

FIG. 8.—– Schematic diagrams of nuclear levels relevant to two-stage neutron (a) absorption and (b) emission, which take place in the matter initially present above a density of about 3×10^{13} g cm^{-3} during the compression and decompression, respectively, due to the spin-down with $P_{\rm rot}(t=0) = 1$ ms. When the Fermi energy of dripped neutrons including the rest mass, $\mu_n + m_n c^2$, crosses the energy threshold, D_{A+1} (D_A), for neutron absorption (emission) by the even-even nucleus (A, Z), the nucleus changes into the next one $(A+1, Z)$ $[(A-1, Z)]$ in a quasi-equilibrium condition. Successively, another neutron absorption (emission) occurs, which in turn releases the energy $qA_{\rm cell}$ in the medium. The resulting state in which the system contains the even-even nucleus stays in quasi-equilibrium. The two-step feature of the reactions described above is attributable to the differences between the values of D_A for odd A and those for even A, which occur due to the nuclear pairing effects.

FIG. 9.—– Changes in the equation of state of zero-temperature matter in the crust from the ground-state one due to the compression. The solid circles show the equilibrium equation of state, and the crosses denote the equation of state of the matter deviated from nuclear equilibrium by an increase of 30% in its pressure. The solid line is the equation of state of BPS.

FIG. 10.—– Heating rates as a function of the age of neutron stars with various values of surface dipole magnetic fields. The initial rotation period $P_{\rm rot}(t=0)$ is taken to be 1 ms.

FIG. 11.—– Photon luminosity from the surface of a neutron star as a function of the spin-down power. The solid line is the bolometric luminosity, $L^H_{\rm bol}$, predicted from the heating rate $H(t)$, and the dashed line is the X-ray (0.1–2.4 keV) luminosity, L^H_X, predicted from $H(t)$ by assuming a blackbody spectrum. For comparison, the X-ray luminosities observed from some millisecond pulsars (Danner et al. 1994) are shown. Triangles denote upper limits; asterisks detections; a diamond a possible detection. The empirical curve (Ögelman 1995; dotted line) for X-ray luminosities coming from the stellar magnetosphere is also plotted.

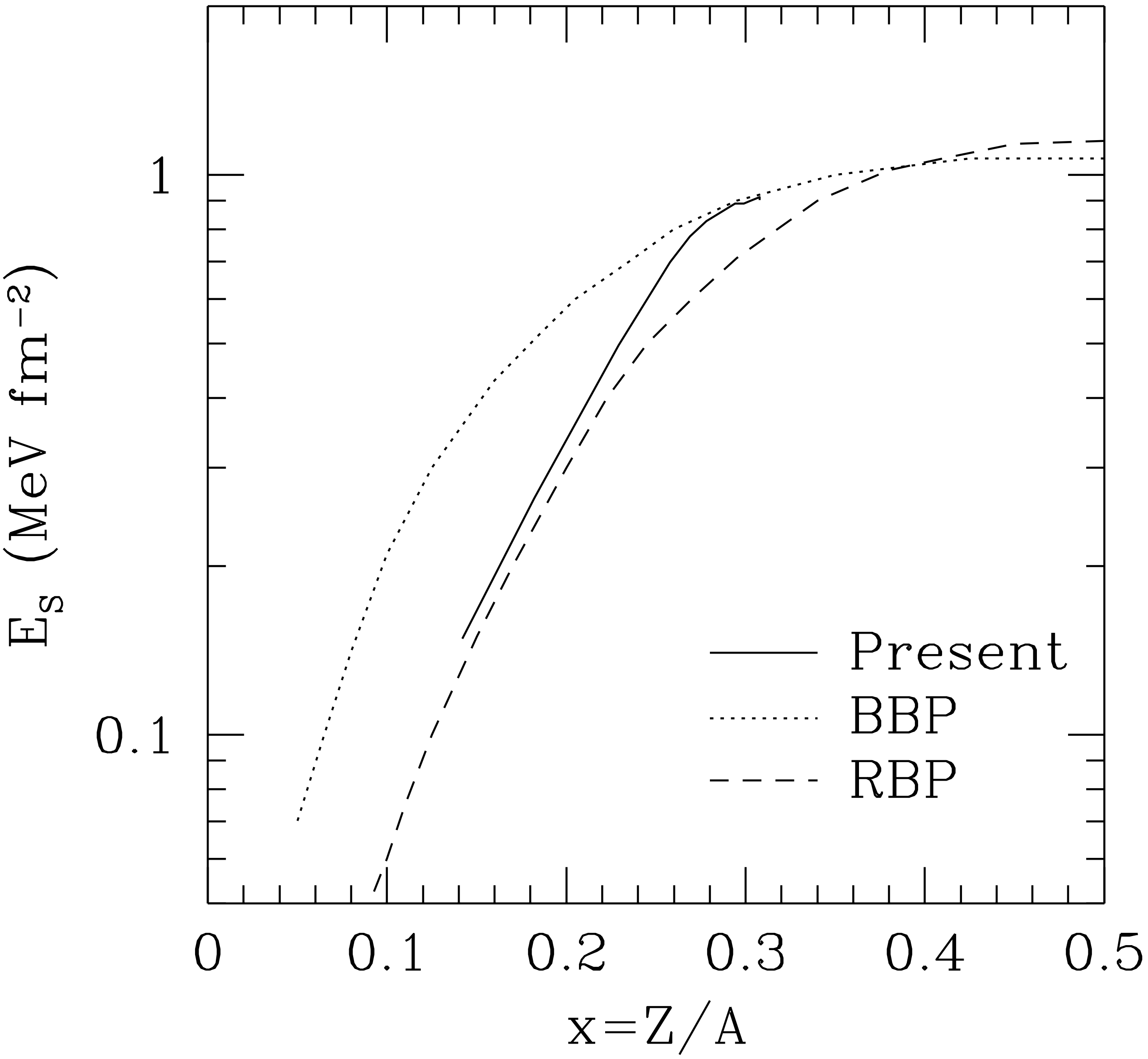

FIGURE 1

IIDA & SATO

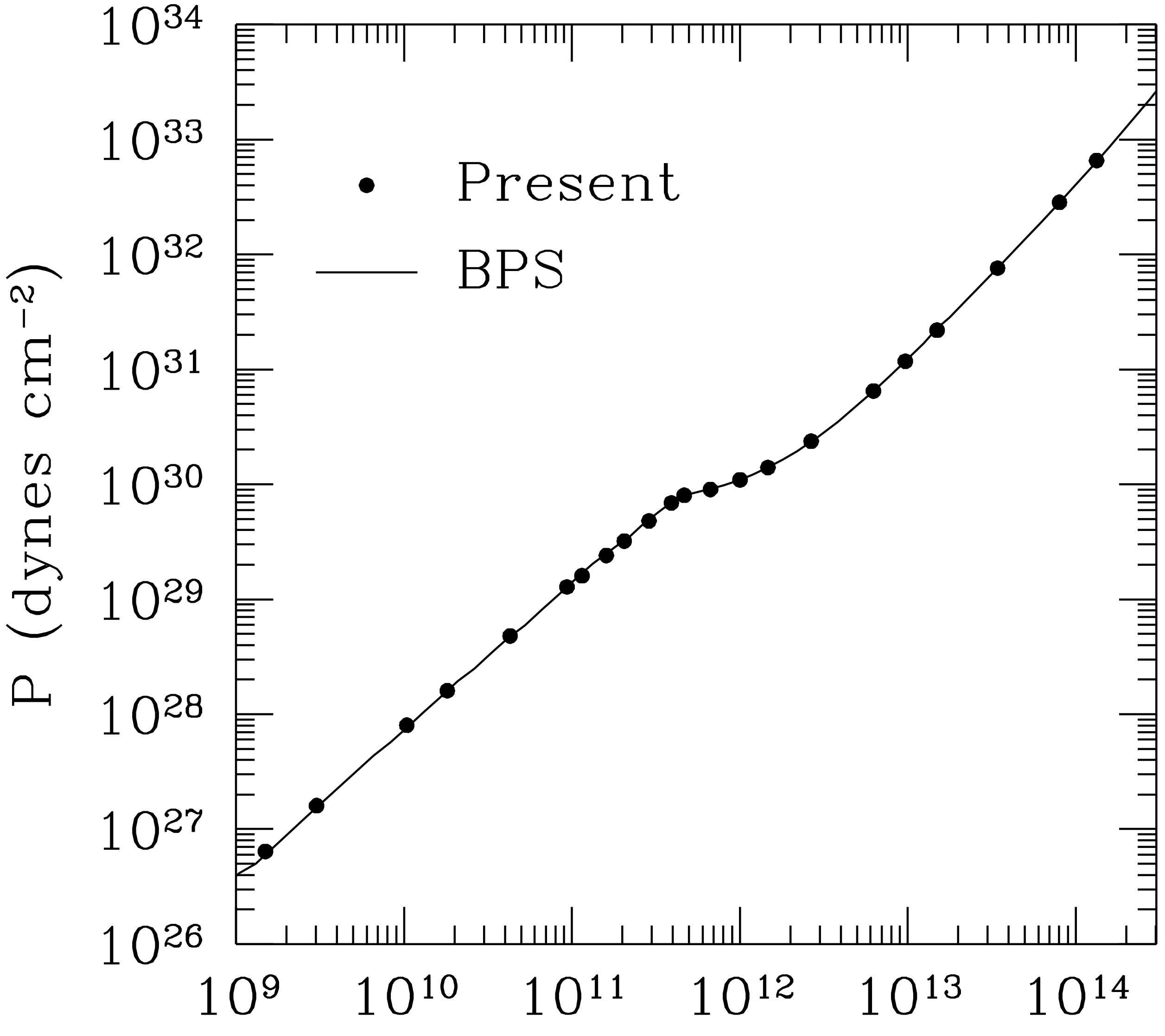

FIGURE 2

IIDA & SATO

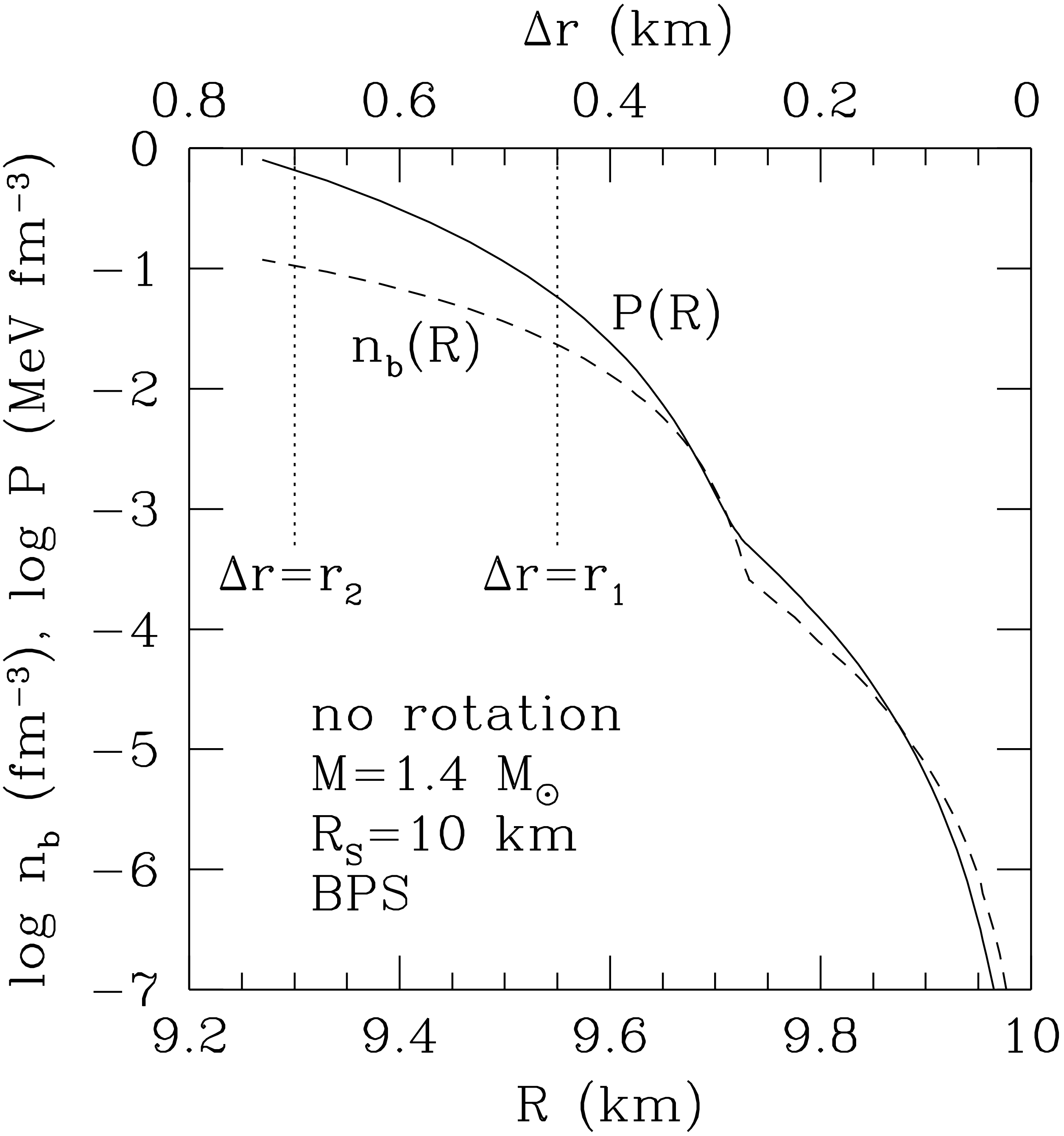

FIGURE 3

IIDA & SATO

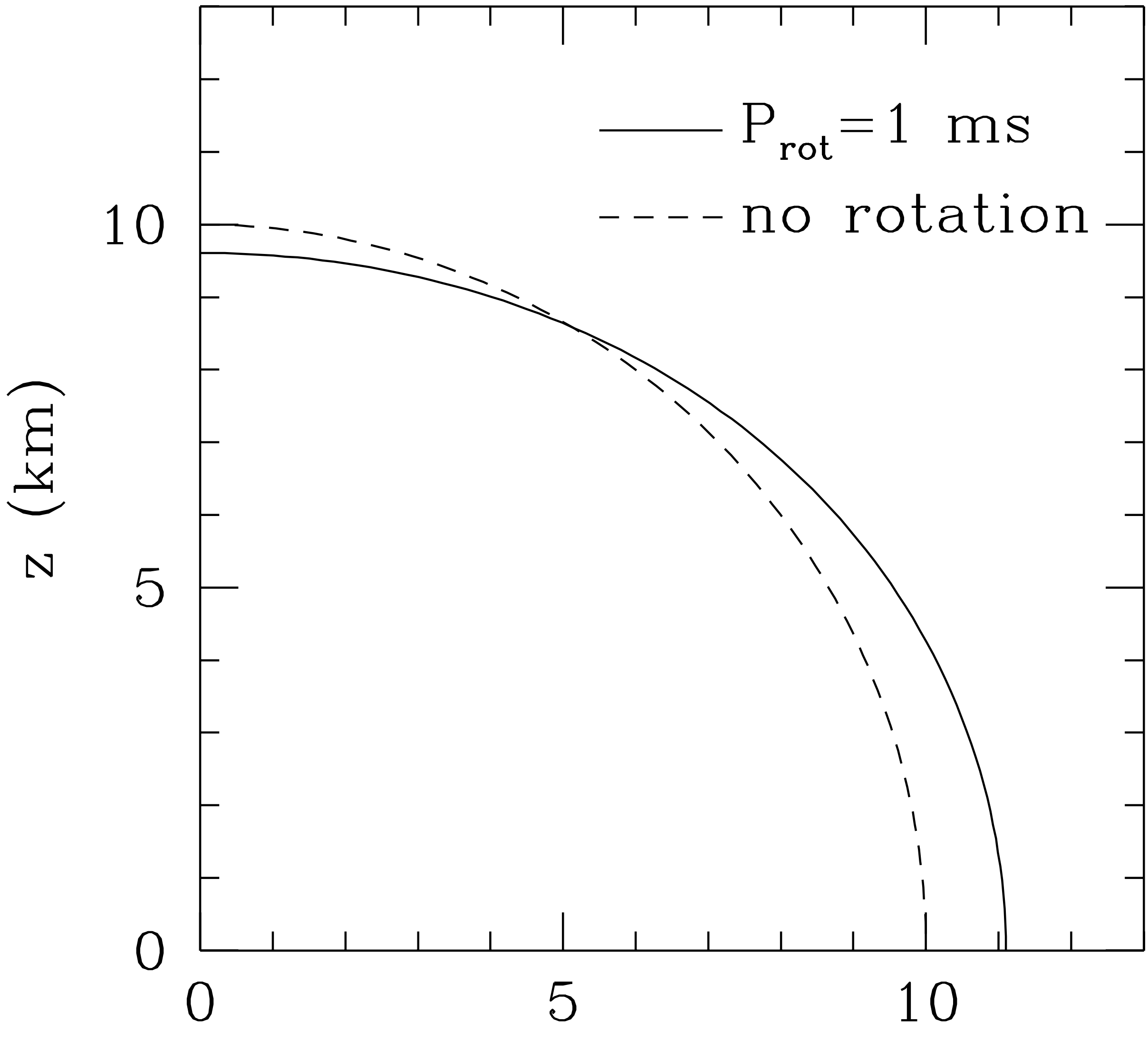

FIGURE 4

IIDA & SATO

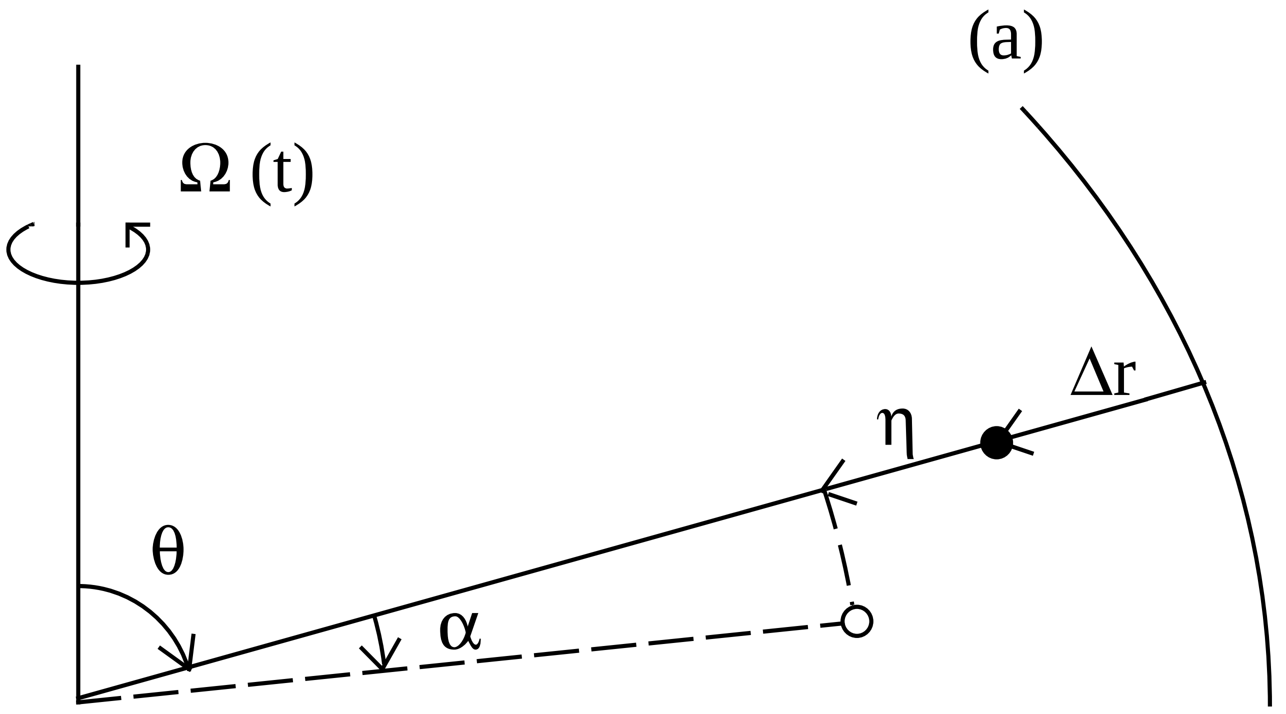

FIGURE 5

IIDA & SATO

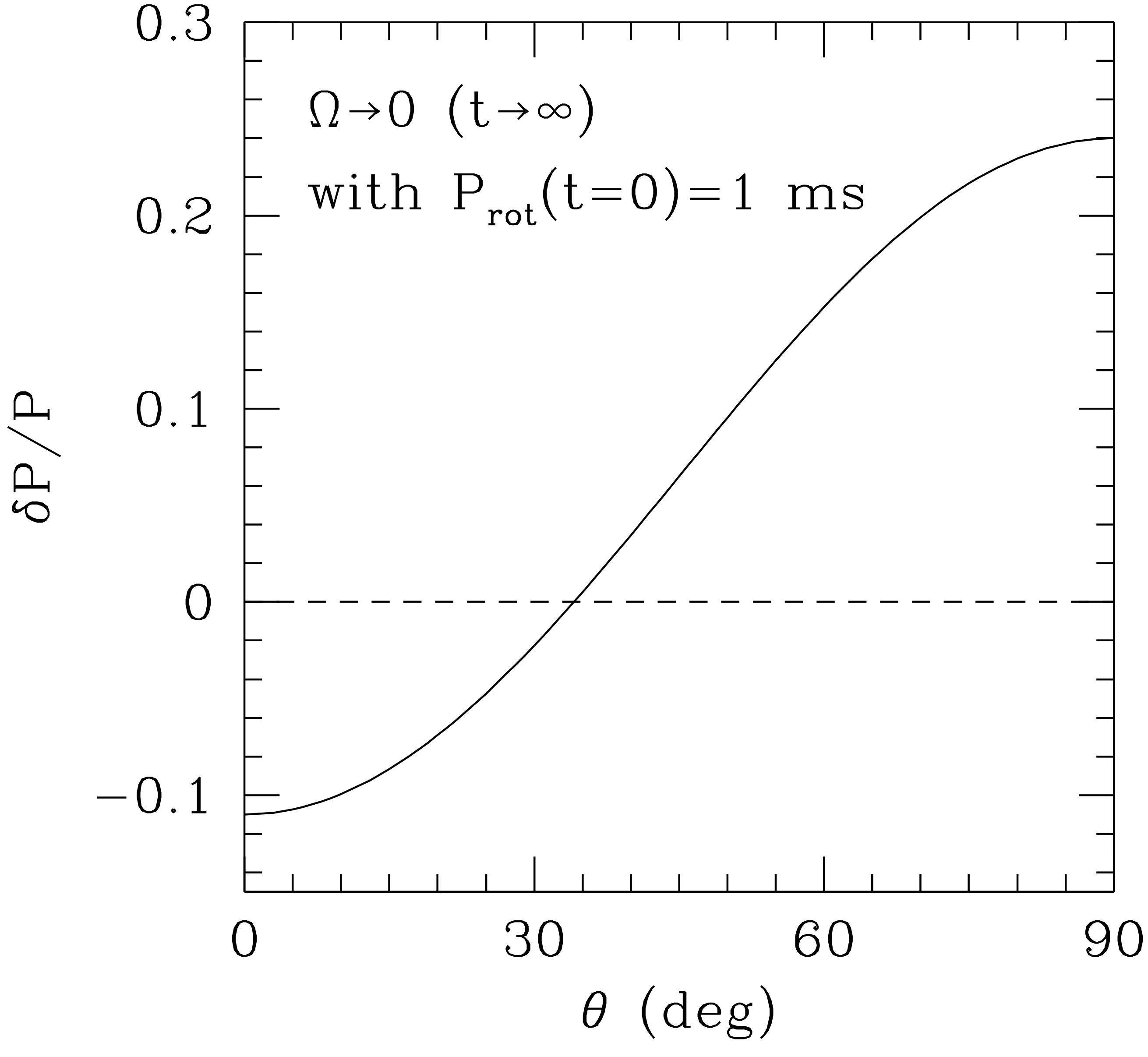

FIGURE 6

IIDA & SATO

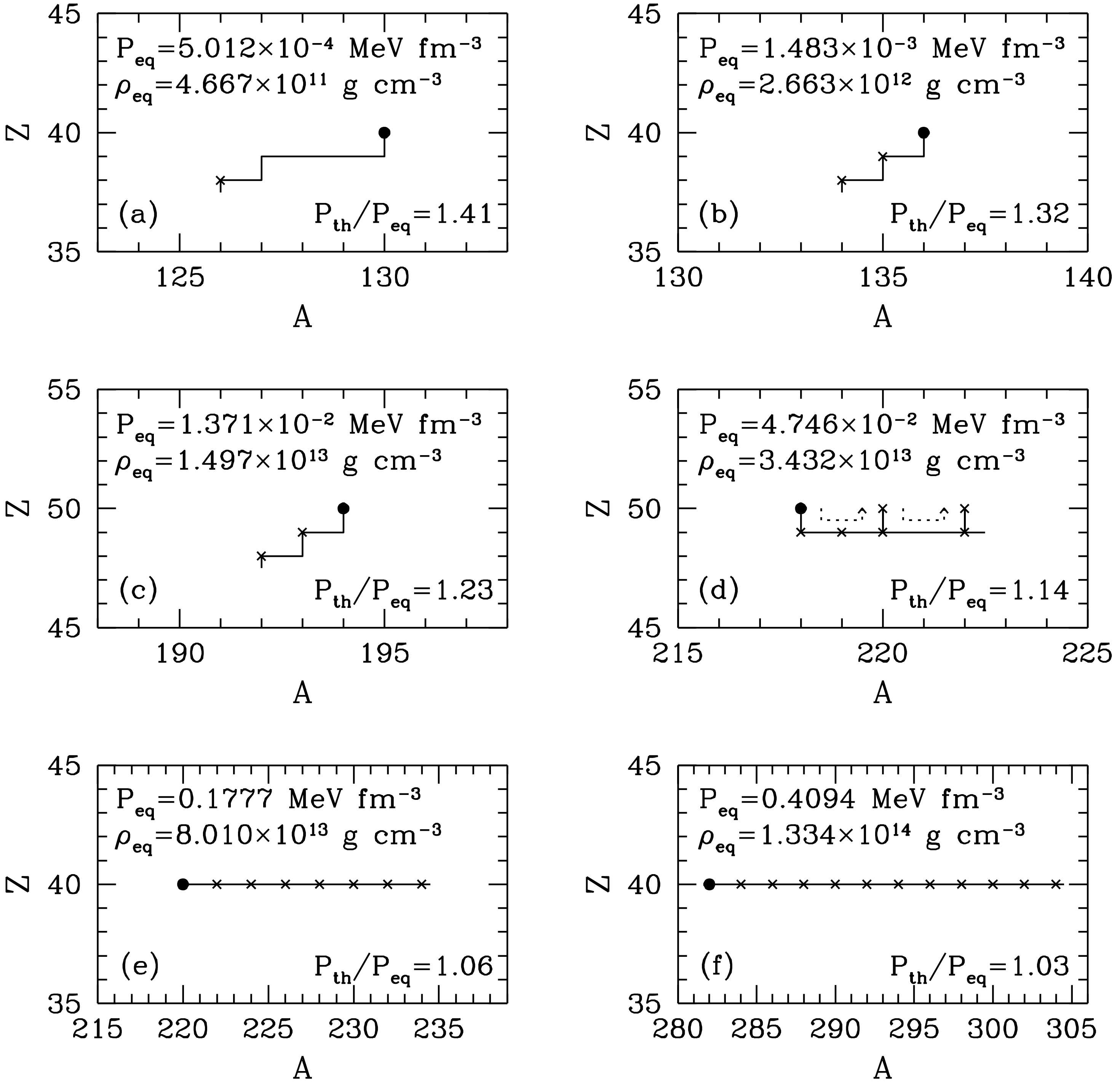

FIGURE 7

IIDA & SATO

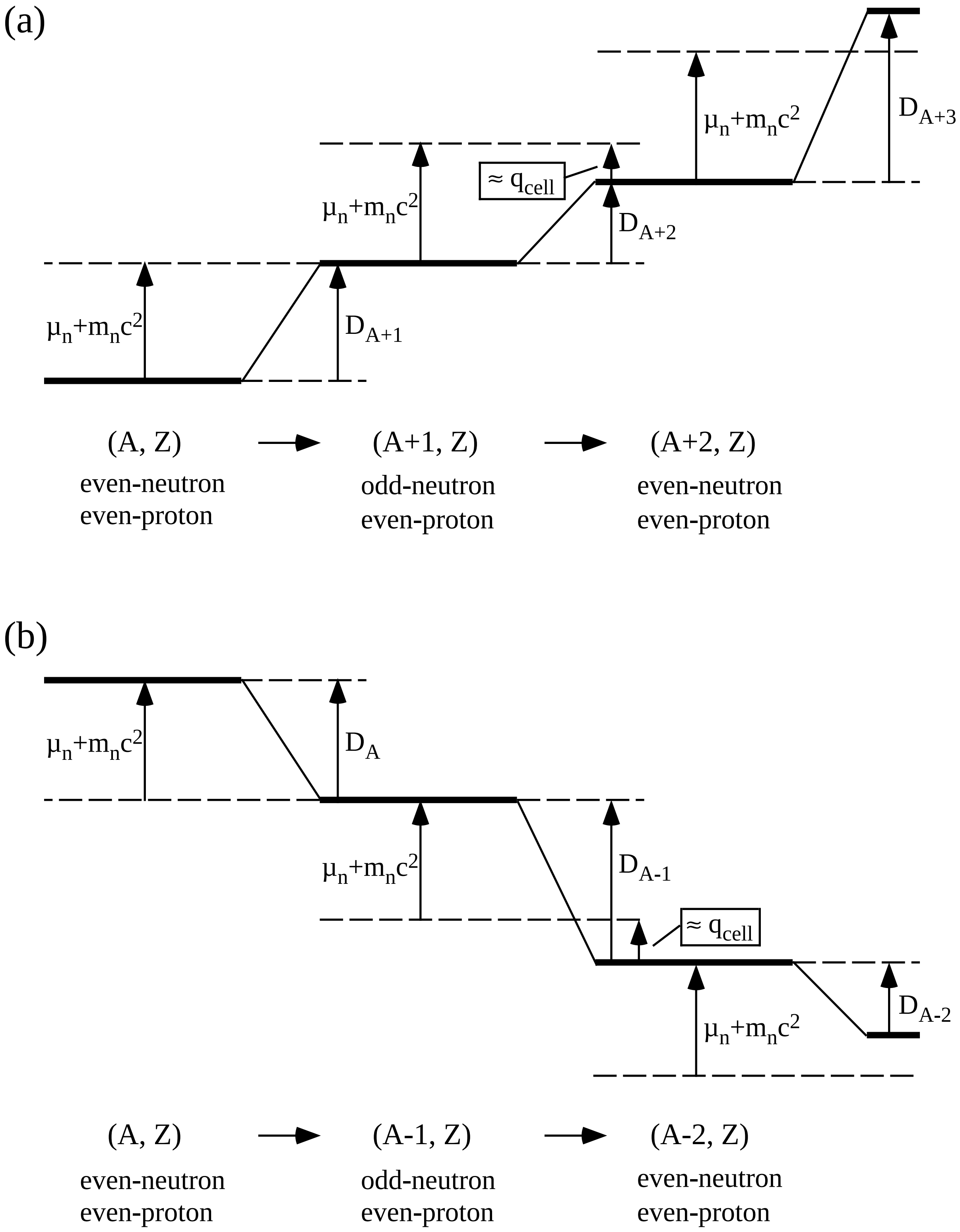

FIGURE 8

IIDA & SATO

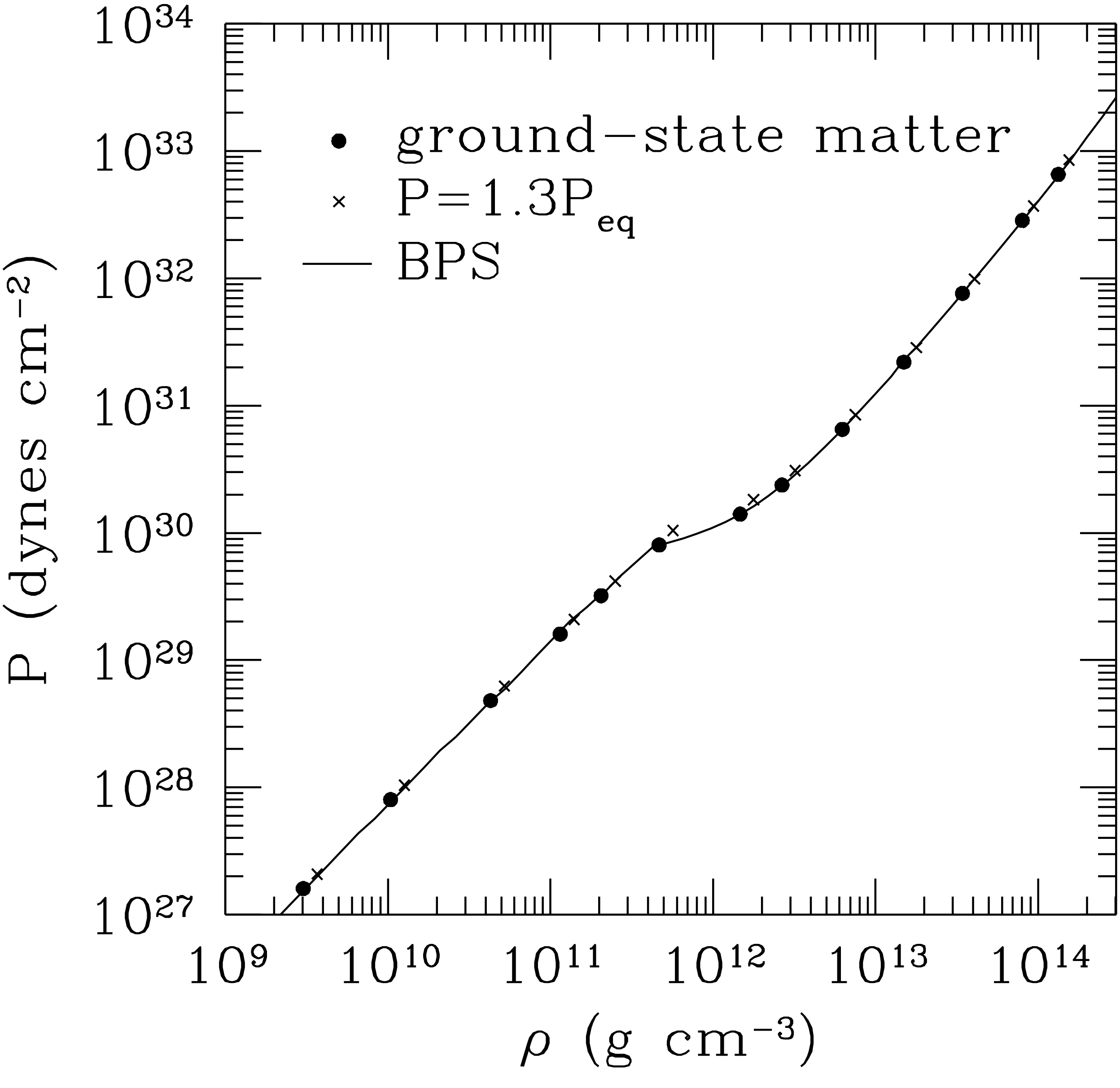

FIGURE 9

IIDA & SATO

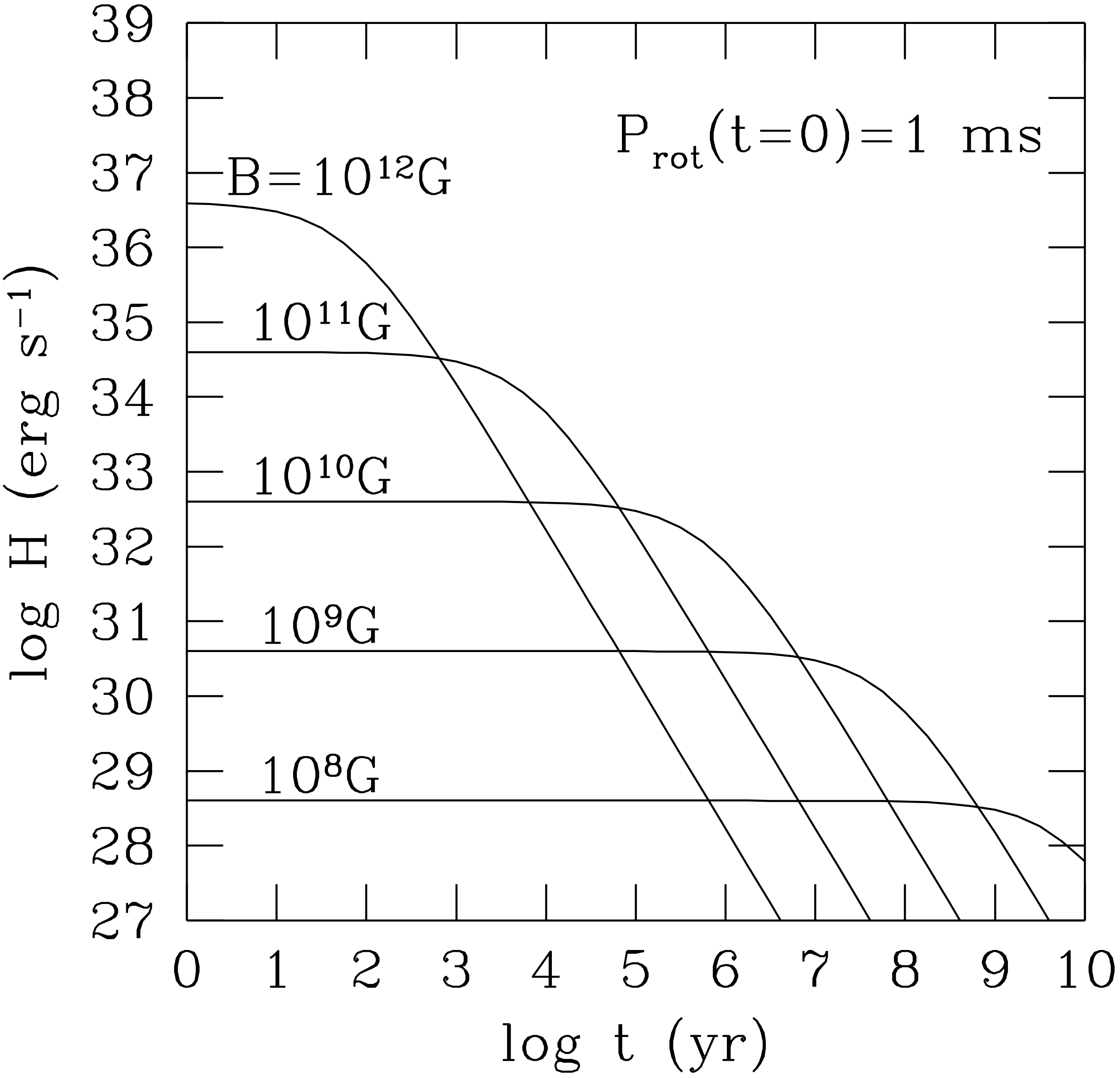

FIGURE 10

IIDA & SATO

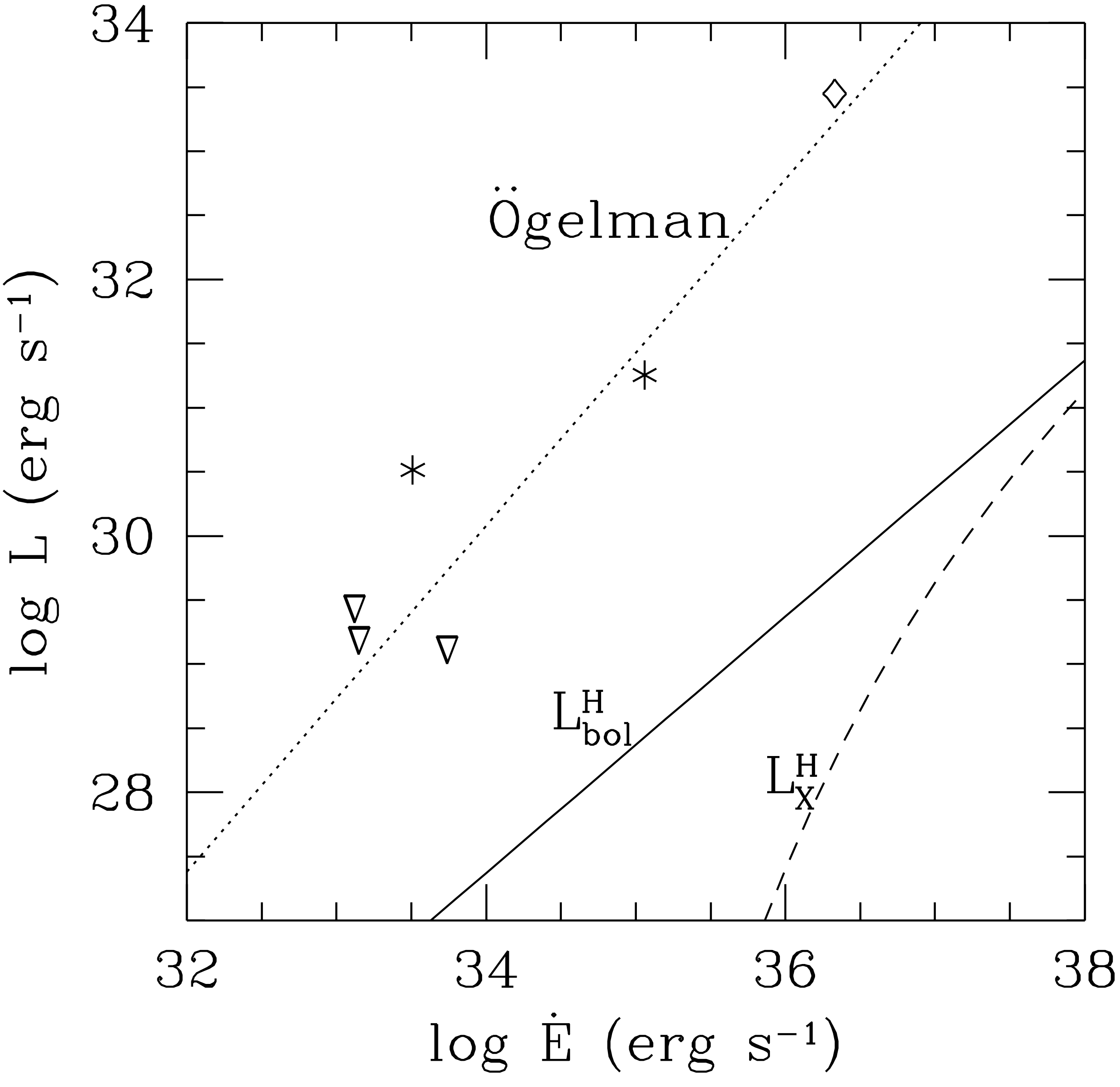

FIGURE 11

IIDA & SATO